7
Supramolecular Architectures Based On Organometallic Half-sandwich Complexes

Thomas B. Rauchfuss and Kay Severin

7.1
Introduction

Cationic half-sandwich reagents have evolved as versatile building blocks that permit controlled growth of stable functional nanostructures. The key half-sandwich modules of interest are cations with the formula $[(\pi\text{-ligand})M]^{n+}$. The most popular derivatizing agents are the dications $[Cp^*M]^{2+}$ (M = Rh, Ir). These half-sandwiches are facial and tritopic, meaning that they have three mutually adjacent points of attachment. The facial arrangement of the sites encourages the formation of molecular structures, whereas meridional tritopic Lewis acids would favor the formation of polymers. In terms of stabilizing nanostructures, the advantages of the half-sandwich components containing cyclopentadienyl ligands are several:

- The large organic ligand partially protects the exterior of the nanostructure with a lipophilic sheath that enhances the solubility of its derivatives, compensating for the low solubility that is often characteristic of large aggregates. Furthermore, bulky C_5Me_5 ligands inhibit polymerization by facilitating intramolecular condensations, giving entropically favored closed structures [1].
- The cyclopentadienyl ligands are virtually inert. This important characteristic is perhaps best demonstrated by the syntheses of $[(C_5R_5)M(CN)_3]^-$ (M = Co, Rh, Ir) and $[(C_5R_5)Ru(CN)_3]^{2-}$, which are generated by treatment of the precursor half-sandwich halides with excess cyanide salt [2].
- The Cp* ligand facilitates characterization of complicated ensembles because it provides a conveniently intense, simple label for ^1H and ^{13}C NMR analysis of complex mixtures and the mass spectra of Cp*M-derived species are relatively simple.
- Cyclopentadienyl ligands can be obtained commercially with diverse substitution patterns; for example, C_5Me_4H and C_5Me_4Et can be readily attached to Rh(III) and Ir(III) to modify usefully the solubility, spectroscopy, crystallizability and geometry of the resulting ensembles.

Organic Nanostructures. Edited by Jerry L. Atwood and Jonathan W. Steed

ISBN: 978-3-527-31836-0

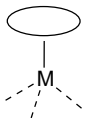

$[(\pi\text{-ligand})M]^{2+}$

$[Cp^*Ru]^+$

$[(C_6Me_6)Ru]^{2+}$

$[(p\text{-cymene})M]^{2+}$ (M = Ru, Os)

$[Cp^*M]^{2+}$ (M = Co, Rh, Ir)

$[(C_4Me_4)Co]^+$

Figure 7.1 Structures of representative half-sandwich units.

Although the above comments are directed to $[Cp^*Rh]^{2+}$ and $[Cp^*Ir]^{2+}$, they also apply to the corresponding $[(C_6R_6)Ru]^{2+}$ derivatives [3]. Additionally, related vertices $[Cp^*Co]^{2+}$, $[CpCo]^{2+}$, $[Cp^*Ru]^+$ and $[(C_4Me_4)Co]^+$ have also received intermittent attention (Figure 7.1) [4].

The $12e^-$ species $[(\pi\text{-ligand})M]^{2+}$ forms unsaturated products upon binding bidentate ligands XY^{n-}. The resulting $16e^-$ species, $[(\pi\text{-ligand})M(XY)]^m$ tend to condense further via the formation of inter-complex donor–acceptor interactions to give $[(\pi\text{-ligand})M(XY)]_x^{mx-}$. The possibility of adjusting the charge of the ensemble allows one to manipulate the strength of both the intermetallic and the host–guest interactions. The power of this design is especially well illustrated by the work involving organic ligands (see Sections 7.2 and 7.3.2).

The half-sandwich reagents $[Cp^*MCl(\mu\text{-Cl})]_2$ are commercially available and readily prepared [5]. The chloro-bridged dimers themselves are conveniently reactive because of the easy scission of the chloride bridges by even weak Lewis bases. The solvated salts, which are often generated *in situ*, represent more potent electrophiles. The salts $[Cp^*Rh(MeCN)_3](PF_6)_2$ and $[(arene)Ru(MeCN)_3](PF_6)_2$ are typical reagents of choice [5]. It is sometimes necessary to generate *in situ* complexes derived from acetone [6] or nitromethane [7] when examining very weakly basic ligands. These salts are prepared by the usual AgCl precipitation methods. Relative to the simple aquo complexes, for example $[Rh(H_2O)_6]^{3+}$, the solvent ligands on the half-sandwich complexes are more labile [3].

7.2 Macrocycles

Rectangular macrocycles with (π-ligand)M complexes in the corner can be obtained by utilization of linear, difunctional ligands such as diisocyanides [8,9], 4,4′-bipyridine [9,10], cyanamide [11] or cyanide [12]. These macrocycles are generally synthesized in a stepwise fashion from the chloro-bridged dimers $[(\pi\text{-ligand})MCl(\mu\text{-Cl})]_2$ [(π-ligand)M = (arene)Ru, Cp*Rh, Cp*Ir]. Three representative examples are shown in Figure 7.2.

An alternative synthesis of macrocycles entails the combination of (π-ligand)M complexes with trifunctional ligands. In this case, two of the donor atoms form a chelate complex with one metal fragment and the remaining donor atom

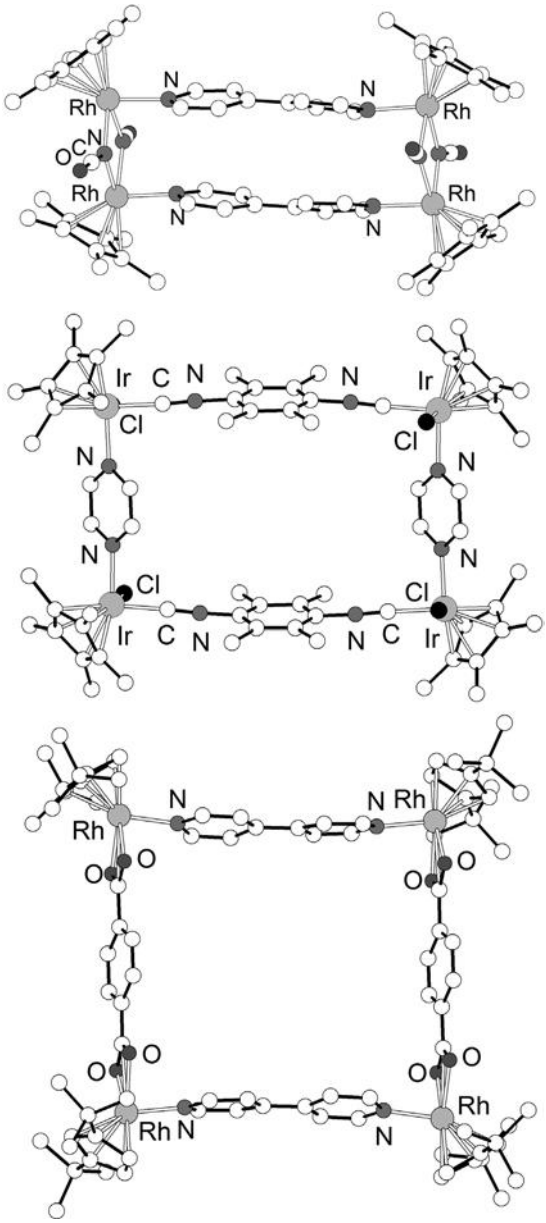

Figure 7.2 Molecular structures of the macrocycles $[(Cp^*Rh)_2(\mu\text{-}NCO)_2(\mu\text{-}4,4'\text{-dipyridyl})]_2(OTf)_4$ (top), $[(Cp^*IrCl)_2(\mu\text{-}C_4H_4N_2)(\mu\text{-}1,4\text{-}(CN)_2C_6Me_4)]_2(OTf)_4$ (middle) and $[\{(1,3\text{-}^tBu_2C_5H_3)Rh\}_2(\mu\text{-}4,4'\text{-dipyridyl})(\mu\text{-terephthalate})]_2(OTf)_4$ (bottom) in the crystal. The hydrogen atoms and the triflate anions are not shown for clarity.

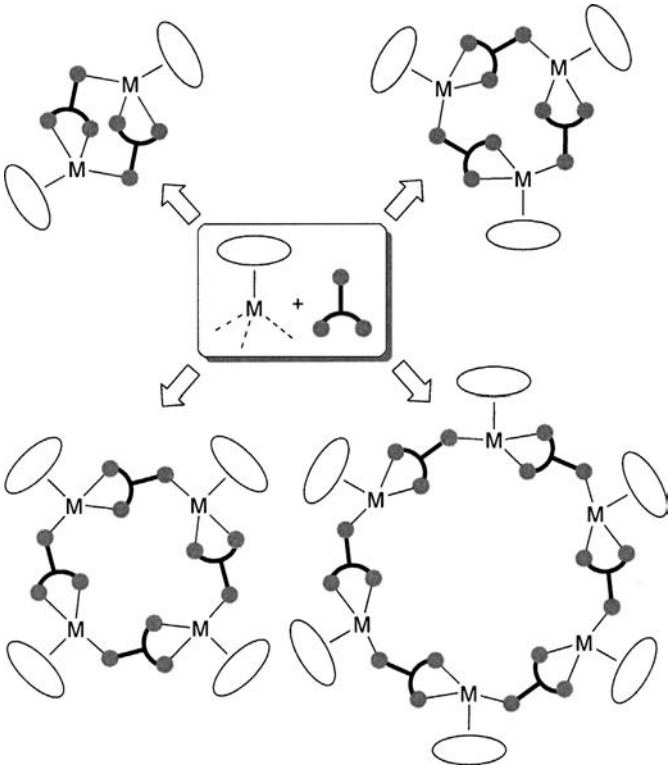

Scheme 7.1 Formation of macrocycles by reaction of organometallic half-sandwich complexes with trifunctional ligands.

coordinates to an adjacent metal fragment. Using this strategy, di-, tri-, tetra- and hexanuclear metallamacrocycles have been obtained (Scheme 7.1).

Cationic complexes comprised of three Cp*Rh fragments connected by three nucleobase derivatives were studied extensively by Fish's group [13]. Structurally related trimers with (arene)Ru^{II}, Cp*Ir^{III} (Figure 7.3) or Cp*Rh^{III} complexes were reported by the groups of Sheldrick [14,15], Yamanari [16] and Vogler [17]. For certain nucleobase ligands, still larger assemblies were observed. Tetranuclear complexes were obtained when adenine [15] or 6-purinethione [18] were used as the bridging ligands and hexanuclear Cp*Rh and Cp*Ir complexes were obtained with the thio derivative 6-purinethione riboside [19].

Amino acidate ligands are also suited to build trimeric organometallic assemblies [20,21]. In this case, the metal fragments are connected via the two carboxylate O atoms and the amino group (Figure 7.3). It is interesting that these trimers can be used as catalysts for the enantioselective hydrogen transfer reactions [21]. The catalytically active species, however, was suggested to be a mononuclear complex.

The macrocycles discussed so far are mostly polycationic species and several of them are soluble in water. In terms of host–guest chemistry, this hydrophilicity

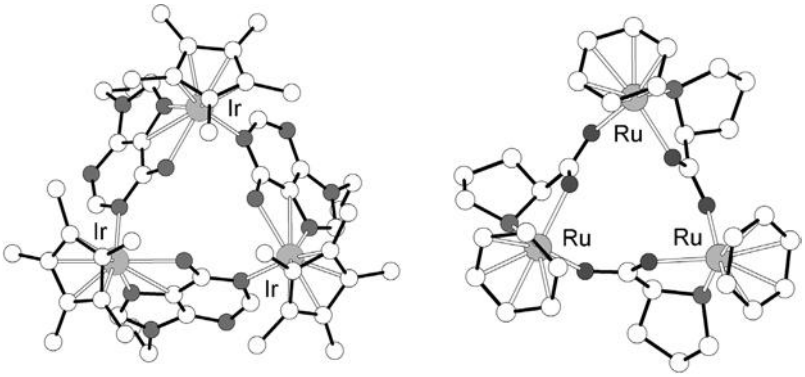

Figure 7.3 Molecular structures of the macrocycles $[Cp^*Ir(L)]_3(OTf)_3$ (L = deprotonated 9-ethyladenine) (left) and $[(p\text{-cymene})Ru(prolinato)]_3(BF_4)_3$ (right) in the crystal. The hydrogen atoms, the side-chains of the *p*-cymene ligands and the counter-anions are not shown for clarity.

may be advantageous if hydrophobic interactions are the main driving force for guest inclusion. Trimeric Cp*Rh complexes, for example, have been shown to act as hosts for aromatic carboxylic acids including amino acids [13e]. Strong complexation-induced chemical shifts were observed in the ^1H NMR spectra. The Cp*Rh trimers may therefore be of interest as ^1H NMR shift reagents [13c].

Macrocyclic complexes with a net charge of zero were obtained with the following ligands: 2,3-dihydroxypyridine (Figure 7.4a) [22,23], 3-acetamido-2-hydroxypyridine [23], 2,3-dihydroxyquinoline [24], 2,3-dihydroxyquinoxaline [24], 6-methyl-2,3-phenazinediol (Figure 7.4b) [24], 3,4-dihydroxy-2-methylpyridine (Figure 7.4c) [25] and 4-imidazolecarboxylic acid (Figure 7.4d) [24]. Using half-sandwich reagents, both trimeric and tetrameric assemblies were generated.

Both the neutral and the cationic macrocycles based on trifunctional ligands are obtained in a highly diastereoselective fashion. Trimeric aggregates were found to adopt a (pseudo)-C_3 symmetric structures with all three metal centers having the same absolute configuration. Resolution of the macrocycles was achieved by using chiral bridging ligands [16] or the chiral guests Li(Δ-TRISPHAT) [26]. Tetrameric aggregates, on the other hand, display a (pseudo)-S_4 symmetry with the metal centers having alternating configurations [15,18,24].

Trinuclear complexes derived from half-sandwich complexes and 2,3-dihydroxypyridine ligands represent organometallic analogues of 12-crown-3 [27]. It was found that these complexes display a very high affinity for lithium and sodium salts (Scheme 7.2) [22,23]. The alkali metal ion M^+ is coordinated to the three adjacent oxygen atoms of the receptor. In the solid state and in apolar organic solvents, the salt MX is bound as an ion pair. Complexation of potassium salts was not observed and this was explained by the steric constraints imposed by the π-ligands.

The affinity of the 12-metallacrown-3 complexes for lithium and sodium salts is remarkably high. Competition experiments with organic ionophores have revealed

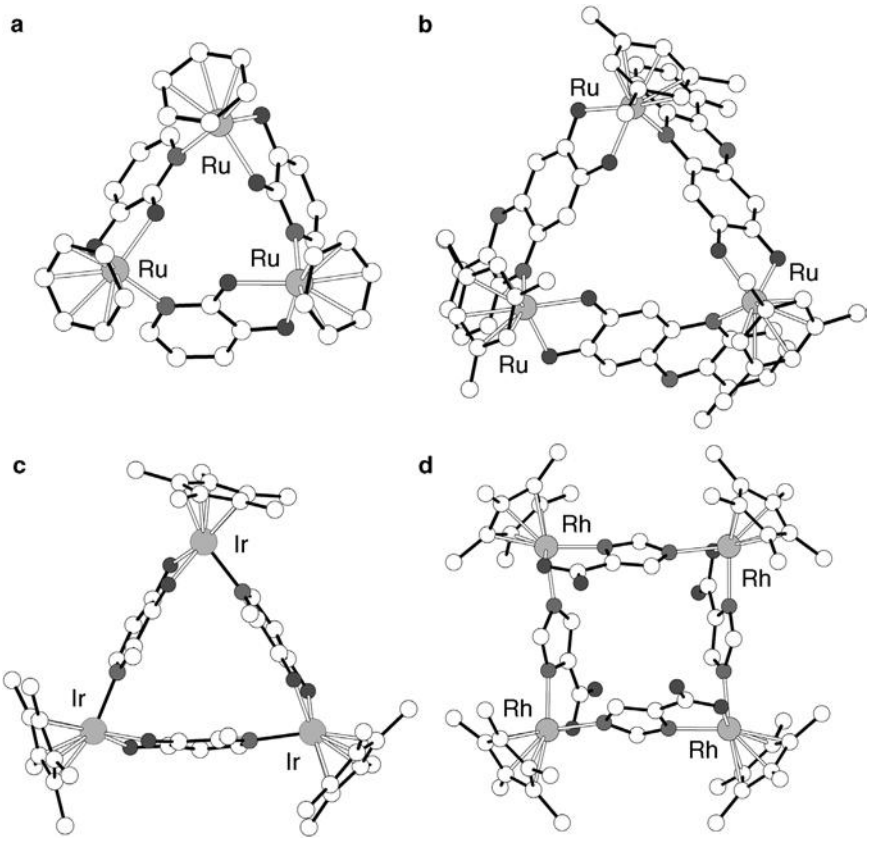

Figure 7.4 Molecular structures of selected organometallic macrocycles in the crystal. They were obtained by combination of (a) (benzene) Ru complexes with 2,3-dihydroxypyridine ligands; (b) (1,3,5-trimethylbenzene)Ru complexes with 6-methyl-2,3-phenazinediol ligands; (c) Cp*Ir complexes with 3,4-dihydroxy-2-methyl-pyridine ligands; and (d) Cp*Rh complexes with 4-imidazolecarboxylic acid ligands. The hydrogen atoms are not shown for clarity.

that in chloroform, the binding affinity for LiCl and NaCl is significantly higher than that of classical crown ethers and comparable to that of cryptands [23]. The high affinity can be attributed to several facts: (a) the receptors are well preorganized to bind lithium or sodium ions; (b) the salts are bound as an ion pair; (c) the energetic costs for the desolvation of the receptors are very low because only one solvent molecule can fit inside the binding cavity; and (d) the oxygen donor atoms display a high partial negative charge [28]. The outstanding affinity of the 12-metallacrown-3 complexes for lithium and sodium salts was utilized to capture molecular LiF [29] and Na_2SiF_6 (Figure 7.5) [30]. It should be noted that the stabilization of these compounds in molecular form represents a challenging task due to the high lattice energy of the salts. 12- Metallacrown-3 complexes have also been investigated for their ability to differentiate between the isotopes $^6Li^+$ and $^7Li^+$ using isotope-selective laser

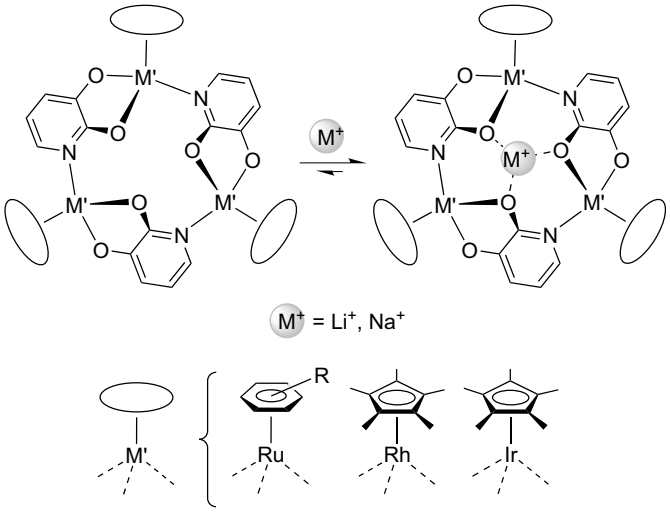

Scheme 7.2 Metallamacrocycles composed of half-sandwich complexes of 2,3-dihydroxypyridine ligands are analogues of 12-crown-3 [(π-ligand)M = (arene)Ru, Cp*Rh, Cp*Ir]. They are able to bind lithium and sodium salts with very high affinity and selectivity.

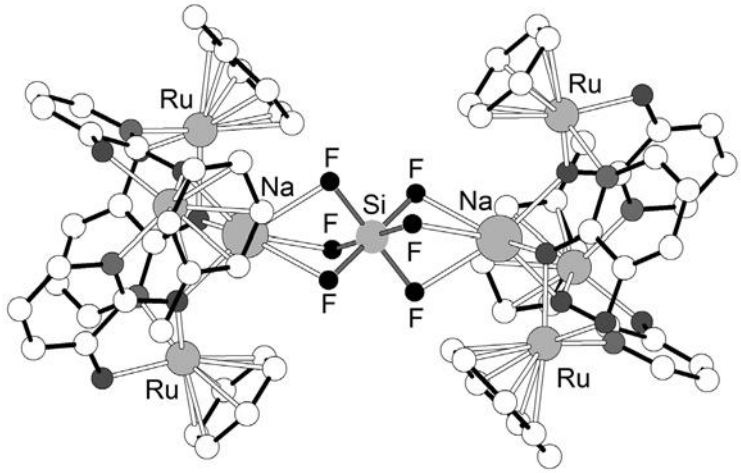

Figure 7.5 Stabilization of molecular Na_2SiF_6 by encapsulation between two [(*p*-cymene)Ru(3-oxo-2-pyridonate)]$_3$ receptors. Hydrogen atoms and the side-chains of the *p*-cymene π-ligands are not shown for clarity.

absorption spectroscopy. It was found that the macrocycle [(C_6Me_6)Ru(3-oxo-2-pyridonate)]$_3$ preferentially binds to the smaller isotope $^7Li^+$ (separation factor α 0.945) [31].

The host–guest chemistry of the trimer [($C_6H_5CO_2Et$)Ru(3-oxo-2-pyridonate)]$_3$ proved to be of special interest. Although this receptor is able to bind Na^+ ions, it shows a very pronounced affinity and selectivity for Li^+ salts as demonstrated in an extraction experiment. When an aqueous solution containing LiCl (50 mM) and a large excess of NaCl, KCl, CsCl, $MgCl_2$ and $CaCl_2$ (each 1 M) was shaken with a chloroform solution of this metallacrown complex, the exclusive and quantitative extraction of LiCl was observed after 24 h [32].

The possibility of obtaining metallacrown complexes with a high specificity for Li^+ is of potential interest for analytical applications, because of the pharmacological importance of lithium salts (Li_2CO_3 is a frequently used drug for patients with bipolar disorder) [33]. To construct Li^+-specific sensors, a receptor that could be used directly in water would be advantageous. To render 12-metallacrown-3 complexes water-soluble, dialkylaminomethyl groups were attached to the bridging 2,3-dihydroxypyridine ligands. With the resulting ligands it is possible to generate macrocycles in water at neutral pH simply by dissolving the aminomethyl-substituted ligand with the corresponding [(π-ligand)MCl_2]$_2$ complex in phosphate buffer. The macrocycles are then formed by self-assembly in quantitative yield [34]. The binding constant for the complexation of Li^+ in water depends on the nature of the (π-ligand)M fragment. With (*p*-cymene)Ru it was possible obtain to a receptor which binds Li^+ with an association constant of $K = 6 \times 10^4\ M^{-1}$ (Figure 7.6) [34a]. This value is sufficient to achieve nearly quantitative complexation of Li^+ at the pharmacologically relevant concentration of ~1 mM. Na^+ ions do not interfere with the complexation because the binding constants are four orders of magnitude lower.

Trimeric macrocycles based on hydroxypyridine ligands were also investigated in the context of dynamic combinatorial chemistry [35]. It was found that macrocycles

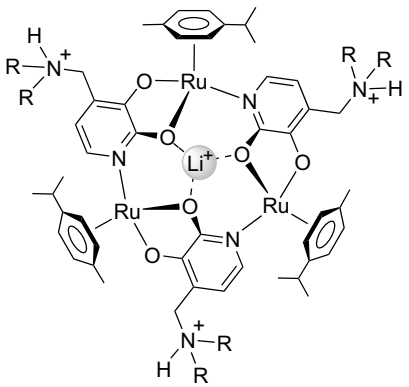

Figure 7.6 Water-soluble 12-metallacrown-3 complexes can be obtained by utilization of 2,3-dihydroxypyridine ligands with dialkylaminomethyl groups. The complexes act as Li^+-specific receptors with binding constants of up to $K = 6 \times 10^4\ M^{-1}$.

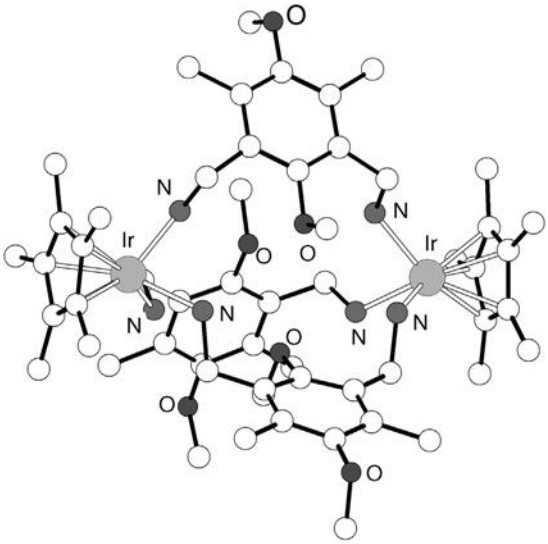

Figure 7.7 Molecular structure of a macrobicyclic Cp*Ir complex with bridging 1,3-bis(aminomethyl)-2,5-dimethoxy-4,6-dimethyl-benzene ligands in the crystal. The hydrogen atoms and the counter-anions are not shown for clarity.

with different (π-ligand)M complexes undergo exchange processes to generate mixed-metal macrocycles [36]. Quantitative analysis of these dynamic equilibria revealed that the product distribution is controlled by steric constraints and can be modulated by addition of guests. These results were used to draw conclusions about the adaptive behavior of dynamic combinatorial libraries in general.

An interesting approach to make *macrobicyclic* organometallic complexes was reported by Amouri's group [37]. They reacted $[Cp^*M(acetone)_3](BF_4)_2$ (M = Rh, Ir) with *m*-xylylenediamine or derivatives as the bridging ligands and obtained cryptand-like structures (Figure 7.7). Some of these complexes tightly encapsulate a BF_4^- anion.

7.3 Coordination Cages

7.3.1 Cyanometallate Cages

The utility of the polymeric cyanometallates was recognized for centuries before the underlying supramolecular chemistry was appreciated [38]. The Hofmann clathrates $\{[Ni(NH_3)_2][Ni(CN)_4](guest)_2\}$ have been used for the size-specific separation of aromatic compounds [39] and Prussian Blue $[Fe_7(CN)_{18}(H_2O)_x]$ and its analogues are versatile dyes [38]. Related coordination compounds and polymers continue to be

topical, because of their potential for the separation of gases [40] and toxic metals [41]. The selectivity of the host–guest behavior of cyanometallates can be attributed in part to the rigidity of the polar framework.

Prussian Blue and its many analogues are derived from the hexacyanometallates, which give rise to three-dimensional polymers [38]. When three of the cyanide ligands are replaced by a π-ligand, the building block retains its ability to form three-dimensional structures but the tendency to polymerize is suppressed. Furthermore, the resulting half-sandwich tricyanides are convenient reagents since, typically as monoanions, they are soluble in a range of nonaqueous solvents. The versatility of the half-sandwich motif is demonstrated by the use of such modules as both the Lewis basic and Lewis acidic components in the synthesis of cyanide-based cages. The prototypical cage complex in this series is $\{[CpCo(CN)_3]_4[Cp^*Rh]_4\}^{4+}$, which forms quantitatively upon combining equimolar amounts of $[CpCo(CN)_3]^-$ and $[Cp^*Rh(MeCN)_3]^{2+}$ (Scheme 7.3) [42]. The cuboidal cage, which has been described as a "molecular box", has idealized T_d symmetry. It is now clear that numerous related boxes can be generated by similar condensations [4]. NMR analysis shows that the condensation proceeds without scission of the Co−CN bonds, thus the building block concept and of course the angles imposed by the box match the coordination preference of the octahedral vertices.

The extensive library of half-sandwich reagents allows one to prepare cyanometallate boxes with a range of charges. The charge on these cages influences the ionophilicity of the resulting cages: anionic and neutral cage are excellent receptors for alkali metal cations. Thus, the condensation of $[CpCo(CN)_3]^-$ and $[Cp^*Ru(NCMe)_3]^+$ and of $[Cp^*Rh(CN)_3]^-$ and $[Mo(CO)_3(NCMe)_3]$ requires the presence of templating cations such as K^+ or Cs^+ [43]. The resulting cages, $\{M\subset[Cp^*Rh(CN)_3]_4[Mo(CO)_3]_4\}^{3-}$ and $\{M\subset[CpCo(CN)_3]_4[Cp^*Ru]_4\}^+$, feature cations inside the cage. The high affinity of these cages for cations arises from the attractive interactions between the π-bonds of the cyanide ligands and the alkali metal cation [44]. Entropy also contributes because encapsulation liberates solvent ligands from

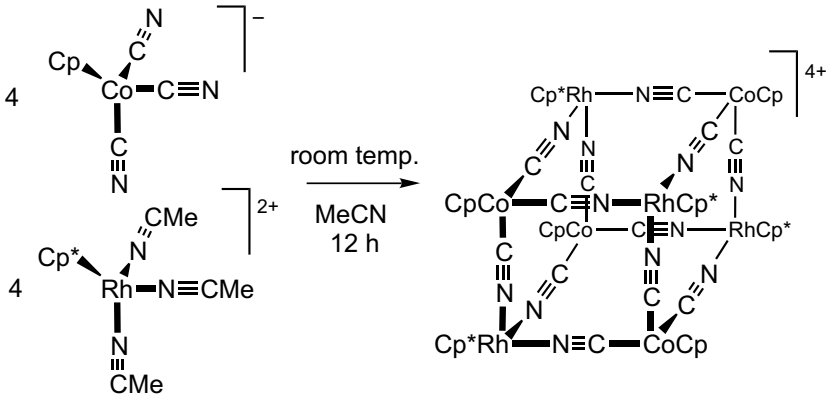

Scheme 7.3 Synthesis of a cyanometallate cage by reaction of $[CpCo(CN)_3]^-$ with $[Cp^*Rh(MeCN)_3]^{2+}$.

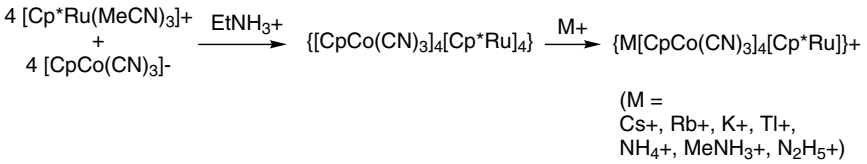

Scheme 7.4 The charge-neutral box $\{[CpCo(CN)_3]_4[Cp^*Ru]_4\}$ acts as a host for cationic guests.

the alkali metal cation in addition to the solvent that is coordinated to the three cationic half-sandwich reagents. The boxes distort upon complexation, but the individual guest–CN interactions are weak, as indicated by long bonds, typically >3.4 Å. Once inside the cyanometallate, the guests are unable to engage in their characteristic reactions. For example, $\{NH_4{\subset}[CpCo(CN)_3]_4[Cp^*Ru]_4\}^+$ is *unreactive* towards D_2O, whereas in solution, of course, NH_4^+ and D_2O exchange protons at diffusion-controlled rates. Ion exchange between included metal ions and those free in solution can also be very slow.

The ion $EtNH_3^+$ templates the formation of $\{[CpCo(CN)_3]_4[Cp^*Ru]_4\}$, a charge-*neutral* box that lacks guests at its interior. The ability of $EtNH_3^+$ to assist in the condensation reflects the strength of the hydrogen bonding interaction $MCN\cdots H^{\delta+}{-}NR_3$. $EtNH_3^+$ is an ideal template because it is highly effective but too large to be contained within the ultimate product. Many ions insert into $\{[CpCo(CN)_3]_4[Cp^*Ru]_4\}$: Cs^+, Rb^+, K^+, Tl^+, NH_4^+, $MeNH_3^+$ and $N_2H_5^+$, to give the corresponding inclusion complexes (Scheme 7.4).

On the basis of kinetic studies, we estimated that the affinity of $\{[CpCo(CN)_3]_4[Cp^*Ru]_4\}$ for Cs^+ is $>10^{10}\,M^{-1}$ [45], which is probably the highest affinity Cs^+ binding agent. Furthermore, the selectivity for Cs^+ in preference to Cs^+ is 10^6.

In no case, however, has this cage been found to bind Na^+, Li^+ or any di- or trivalent ion. These smaller cations are apparently unable to bind simultaneously to sufficient Co*CN*Ru sites to compensate for their desolvation required by the inclusion process. This selectivity highlights the remarkable rigidity of these container molecules. Smaller tetrahedral or trigonal prismatic cages are effective for these small ions, an example being $\{Na[Mo(CO)_3]_4(CN)_6\}^{5-}$ [46].

7.3.1.1 Electroactive Boxes

The Co(I)-containing building block $[Cb^*Co(NCMe)_3](PF_6)$ ($Cb^* = \eta^4$-C_4Me_4) is intriguing because its cage derivatives are susceptible to redox reactions. Condensation of $[Cb^*Co(NCMe)_3]PF_6$ and $K[(C_5R_5)M(CN)_3]$ [$(C_5R_5)M$ = CpCo, Cp*Rh] affords $\{K{\subset}[(C_5R_5)M(CN)_3]_4[Cb^*Co]_4\}^+$ [47]. Once again, the success of the condensation depends on the presence of a cation, otherwise one obtains insoluble polymeric solids. The structure of $\{K{\subset}[CpCo(CN)_3]_4[Cb^*Co]_4\}(PF_6)$ reveals that eight of the Co−CN−Co linkages are bent towards the K^+ guest and the remaining four Co−CN−Co edges relieve this distortion by bowing away from the cage interior (Figure 7.8). This all-cobalt cage can be oxidized with ferrocenium to give the tetracationic derivative concomitant with release of the alkali metal guest. In principle, other half-sandwich receptors could be made switchable electrochemically. Also

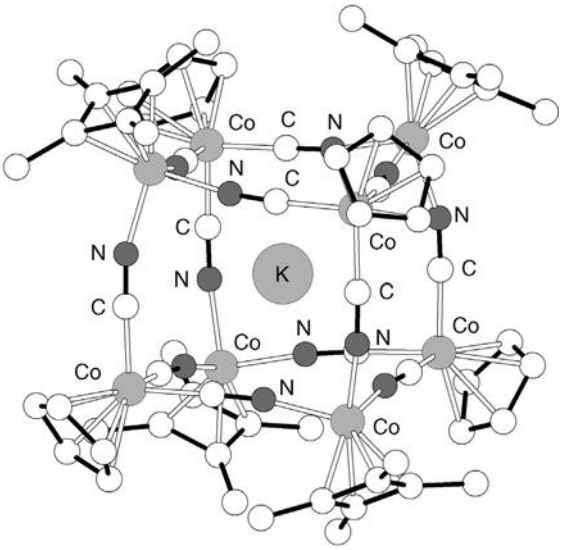

Figure 7.8 Molecular structure of $\{K\subset[CpCo(CN)_3]_4[Cb^*Co]_4\}^+$ in the crystal. The hydrogen atoms are not shown for clarity.

intriguing, the redox potential of the cage complex depends on the nature of the alkali metal, thus indicating that such cages could be used as electrochemical sensors for alkali metal cations.

7.3.1.2 Defect Boxes $\{[(C_5R_5)M(CN)_3]_4[Cp^*M]_3\}^z$

Condensation of $[Cp^*Rh(CN)_3]^-$ and $[Cp^*Rh(NCMe)_3]^{2+}$ affords exclusively the seven-vertex cage $[(Cp^*Rh)_7(CN)_{12}]^{2+}$ [48]. This type of cage, which is better described with the formula $\{[Cp^*Rh(CN)_3]_4[Cp^*Rh]_3\}^{2+}$, is called a "defect box," because it is related to the eight-vertex boxes by removal of one Cp*M vertex. Unlike the $M_8(CN)_{12}$ boxes, however, defect boxes have three terminal cyanides. The stereochemistry of these cyanide ligands is strongly influenced by the presence of a guest at the cage interior. Formation of $\{[Cp^*Rh(CN)_3]_4[Cp^*Rh]_4\}^{4+}$ is prevented by inter-Cp* steric interactions. Even in the absence of strong steric forces, the defect-box motif is kinetically favored relative to the box. Thus, condensation of $[CpCo(CN)_3]^-$ and $[Cp^*Rh(NCMe)_3]^{2+}$ in a 4 : 3 ratio gives $\{[CpCo(CN)_3]_4[Cp^*Rh]_3\}^{2+}$. In these dicationic Rh_7 and Co_4Rh_3 cages, the three terminal cyanide ligands are exocyclic, i.e. they radiate away from the open vertex to give the cage idealized C_{3v} symmetry. In order to convert $\{[CpCo(CN)_3]_4[Cp^*Rh]_3\}^{2+}$ into the box $\{[CpCo(CN)_3]_4[Cp^*Rh]_4\}^{4+}$, the three exocyclic cyanide ligands must reorient, so the final step in box formation is slow.

Condensations of $[CpCo(CN)_3]^-$ with <1 equiv. of the monocationic Lewis acid Cp^*Ru^+ affords defect boxes, but only in the presence of Cs^+, which occupies the interior of the cage (Figure 7.9). In solution, the resulting cage, $\{Cs\subset[CpCo(CN)_3]_4[Cp^*Ru]_3\}$, exists as a pair of interconverting isomers: one has two exo terminal cyanides and the other has one exo terminal cyanide. The "endo" terminal CN groups bind to Cs^+ using their C−N π-bonds [43].

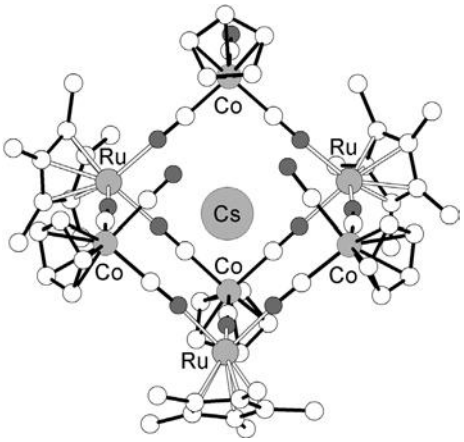

Figure 7.9 Molecular structure of $\{Cs\subset[CpCo(CN)_3]_4[Cp^*Ru]_3\}$ in the crystal. The hydrogen atoms are not shown for clarity.

The species $\{Cs\subset[CpCo(CN)_3]_4[Cp^*Ru]_3\}$ is a versatile triaza ligand, similar in denticity and binding preferences to tris(pyrazolyl)borates and triazacyclononane. It is a rare example of a ligand that contains an alkali metal. In binding the eighth metal, the exo cyanide ligands in $\{Cs\subset[CpCo(CN)_3]_4[Cp^*Ru]_3\}$ reorient to the endo orientation, but this reaction is very fast and obviously intramolecular. Thus, upon treatment with tritopic Lewis acids, $\{Cs\subset[CpCo(CN)_3]_4[Cp^*Ru]_3\}$ efficiently affords heteronuclear boxes $\{Cs\subset[CpCo(CN)_3]_4[Cp^*Ru]_3ML_n\}^z$, where, for example, $ML_n^z = RuH(PPh_3)_2$ and $[CuPPh_3]^+$. With weakly solvated metal cations, double boxes form with the formula $\{Cs\subset[CpCo(CN)_3]_4[Cp^*Ru]_3\}_2M\}^{n+}$ ($M = Na^+$, Fe^{2+}, Ni^{2+}; Scheme 7.5) [43,49].

Particularly instructive were experiments on the corresponding all-Cp* anion-binding defect box $\{M\subset[Cp^*Rh(CN)_3]_4[Cp^*Ru]_3\}$ ($M = Cs^+$ or NH_4^+). Because all vertices carry the Cp* ligand, these cages enjoy enhanced solubility in organic solvents, which in turn has allowed us to monitor cage formation by *in situ* electrospray ionization mass spectrometry (ESI-MS). Such ESI-MS measurements revealed the intermediacy of $CsRh_3Ru_2$ and $CsRh_2Ru_2^+$ clusters, consistent with a role of the alkali metal cation in guiding the assembly of the cage [50]. Because of their more open architecture, the defect boxes exchange guest ions more rapidly than the related ionophilic boxes [50]. Furthermore, the affinity of $\{NH_4\subset[Cp^*Rh(CN)_3]_4[Cp^*Ru]_3\}$ for Cs^+ dwarfs that of the best organic complexant, calix[4]arene-bis(benzocrown-6) (BC6B):

$$CsBC6B^+ + \{NH_4\subset[Cp^*Rh(CN)_3]_4[Cp^*Ru]_3\} \rightarrow \{Cs\subset[Cp^*Rh(CN)_3]_4[Cp^*Ru]_3\}\ NH_4BC6B^+$$

7.3.2
Expanded Organometallic Cyano Cages

The versatility of the CN^- group as a linker ligand has encouraged a search for related building blocks that could stabilize nanoscale architectures. Ishii's group has

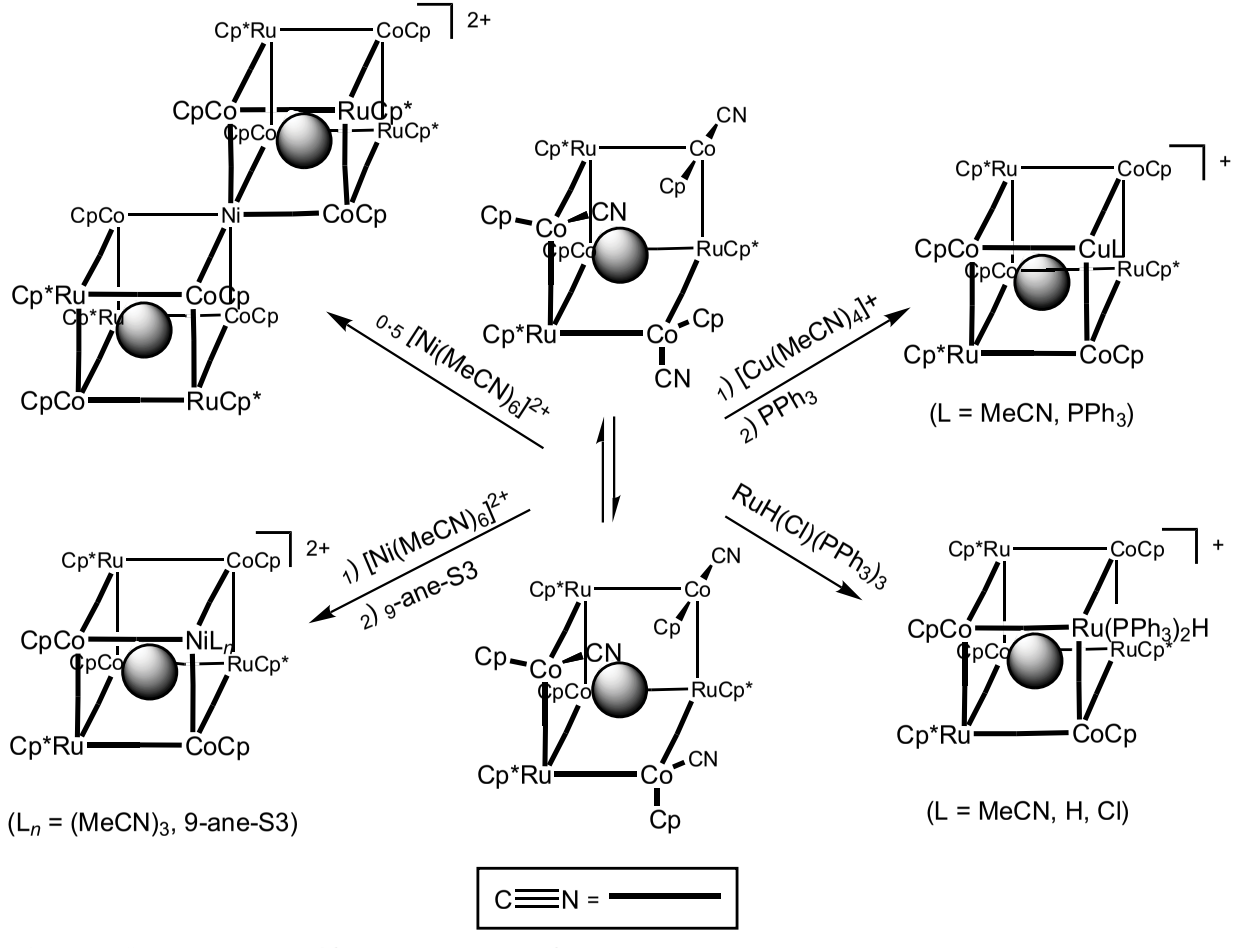

Scheme 7.5 Illustrative reactions of {Cs[CpCo(CN)$_3$]$_4$[Cp*Ru]$_3$}.

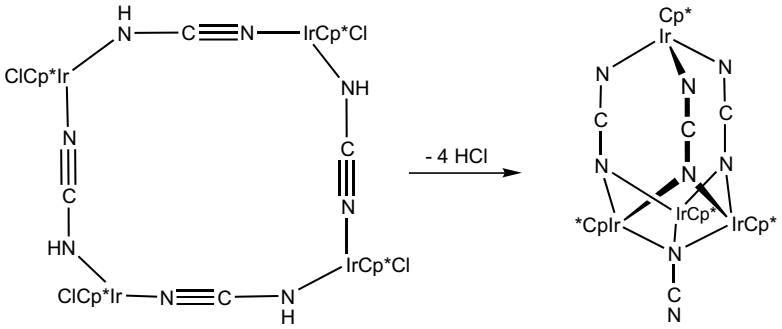

Scheme 7.6 Condensation of an expanded tetrametallic cage via dehydrohalogenation of a cyanamide-linked ring.

shown that cyanamide dianion NCN^{2-} and the related monoanion $NCNH^{-}$ in combination with half-sandwich building blocks affords a variety of novel cage structures [11]. Thus, treatment of NaNCNH with $[Cp^*IrCl_2]_2$ affords $[Cp^*IrCl(\mu_2\text{-NCNH-}N,N')]_4$ consisting of 16-membered macrocycle $[IrNCN]_4$ cores. Dehydrohalogenation converts these rings into elongated cubanes (Scheme 7.6).

The $M_8(CN)_{12}$ boxes have internal volumes that are ideal for the selective binding of very small ions. The scope for host–guest behavior would be greater for larger cages and the possibility of such expanded cyanometallate cages is increasingly apparent. Beltran and Long have described "FCC" boxes wherein the eight tritopic metals are connected via $[M(CN)_4]^{2-}$ linkers that cap each of the eight faces of the expanded box [51]. Another expanded cyanometallate derives from the formal self-condensation of $[Cp^*WS_3(CuCN)_3]^{-}$ and $[Cp^*WS_3Cu_3]^{2+}$. Again, obtaining pure samples has proven to be challenging, but the framework of the new box $\{[Cp^*WS_3Cu_3]_8(CN)_{12}\}^{4+}$ was characterized crystallographically [52]. The size of this container molecule is indicated by its contents: 4 Li^+*and* 8 Cl^-.

Half-sandwich tricyanides enforce box-like structures by their orthogonal NC−M−CN angles and the inertness of the M−CN bonds, which precludes more drastic structural rearrangements. The organoboron tricyanides with the formula $[RB(CN)_3]^{-}$ are well suited as building blocks because they are basic and available with a range of R groups. Because the NC−B−CN angle is more open, these species give rise to cages that are larger than cubes, such as the hexagonal prismatic $\{[PhB(CN)_3]_6[Cp^*Rh]_6\}^{6+}$ (Figure 7.10) [53].

7.3.3
Cages Based on *N*-Heterocyclic Ligands

Trifunctional *N*-heterocyclic ligands can be used to build not only macrocycles but also coordination cages. The basic requirement is that the three donor atoms are not able to form chelate complexes. When the Ru complex $[(p\text{-cymene})Ru(NO_2)_2]$ was mixed with the trifunctional ligand 3,5-pyridinedicarboxylic acid in water, an orange

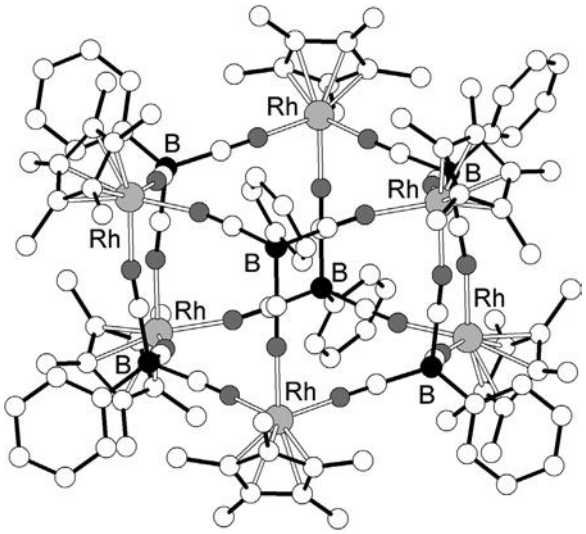

Figure 7.10 Molecular structure of $\{[PhB(CN)_3]_6[Cp^*Rh]_6\}^{6+}$. The hydrogen atoms, the counter-anion and the THF molecule in the cavity are not shown for clarity.

precipitate was formed. This complex turned out to be a hexanuclear cage, in which the (*p*-cymene)Ru fragments are connected by the 3,5-pyridinedicarboxylate ligands (Scheme 7.7) [54]. A related Cp*Ir complex can be obtained from $[Cp^*Ir(OAc)_2]$ and 3,5-pyridinecarboxylic acid in methanol [55].

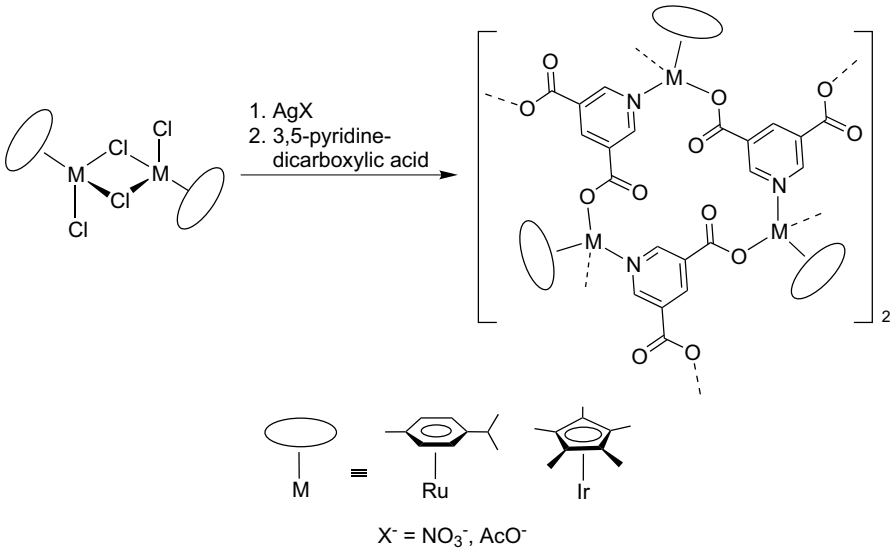

Scheme 7.7 Synthesis of hexanuclear cage complexes with bridging 3,5-pyridinedicarboxylate ligands.

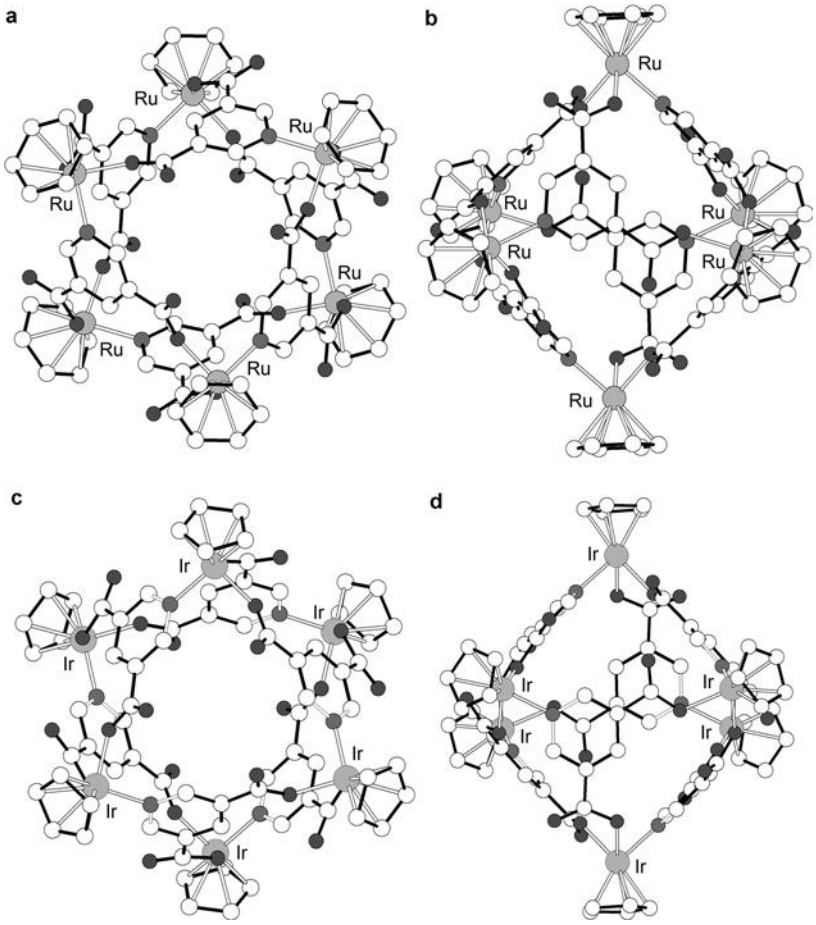

Figure 7.11 Molecular structure of a hexameric (*p*-cymene)Ru complex [(a) view from the top; (b) view from the side] and a hexameric Cp*Ir complex [(c) view from the top; (d): view from the side] in the crystal. The hydrogen atoms, the co-crystallized solvent molecules and the side-chains of the π-ligands are not shown for clarity.

The structures of the hexanuclear cages [(*p*-cymene)Ru(3,5-pyridinedicarboxylate)]$_6$ and [Cp*Ir(3,5-pyridinedicarboxylate)]$_6$ are closely related (Figure 7.11). Each 3,5-pyridinedicarboxylate ligand is coordinated to three different metal atoms via the carboxylate O atoms and the pyridine N atom. The Ru or Ir atoms are positioned in the corner of an octahedron. Metal atoms in opposite corners are 12 Å apart from each other.

The Ru cage was found to act as an exo-receptor for alkali metal ions such as K^+ and Cs^+ [54]. This transformation was evidenced by NMR titration experiments with KOAc or CsOAc in CD_3OD solution. These salts induce a rearrangement of the

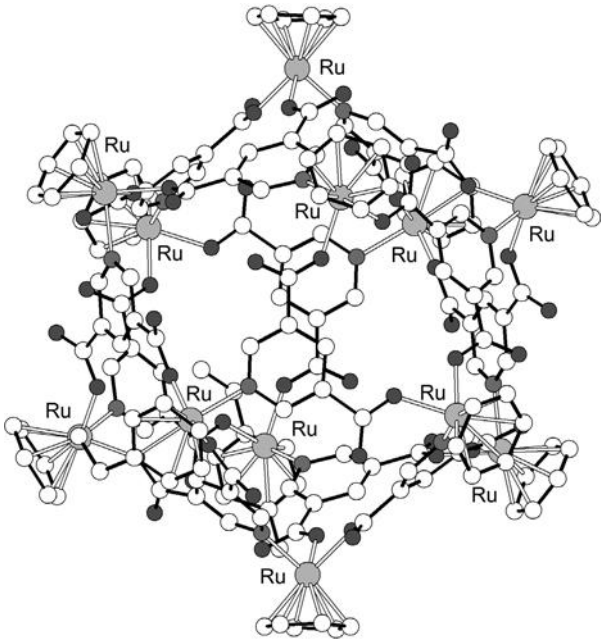

Figure 7.12 Molecular structure of a dodecanuclear (*p*-cymene) Ru complex in the crystal. The hydrogen atoms, the co-crystallized KOAc and solvent molecules and the side-chains of the π-ligands are not shown for clarity.

hexanuclear complex into a dodecanuclear cage (Figure 7.12). The connectivity of the hexa- and dodecanuclear complexes is similar: each (cymene)Ru^{2+} fragment is coordinated to three different heterocyclic ligands via two carboxylates and one pyridine N-atom. The symmetry-related Ru atoms in opposite corners of the cage are separated by 16 Å giving a cavity of approximately 1100 $Å^3$. The icosahedral geometry adopted by this cage resembles the geometry of natural cage structures such as spherical viruses. Twelve of the 20 faces of the icosahedra are occupied by the bridging 3,5-pyridinecarboxylate ligands. The remaining eight faces are surrounded by three carbonyl groups that constitute a metal binding site. Indeed, in the crystal, all eight sites are occupied by K^+ ions (not shown in Figure 7.12). These K^+ centers are coordinated to acetate anions, which interconnect the icosahedra in the crystal. The binding sites for K^+ and Cs^+ are sufficiently better in the dodecanuclear cage to compensate for the entropically disfavored condensation of two hexanuclear cages.

The synthesis of trigonal prismatic cages based on (arene)Ru complexes and bridging 2,4,6-tripyridyl-1,3,5-triazine (tpt) ligands has been investigated by Therrien's group [56,57]. When the dinuclear oxalate complexes [{(*p*-cymene)$RuCl\}_2(C_2O_4)$] or [{$(C_6Me_6)RuCl\}_2(C_2O_4)$] were reacted with 6 equiv. of AgOTf and 2 equiv. of tpt, cationic metallo-prisms were obtained (Scheme 7.8) [56]. The

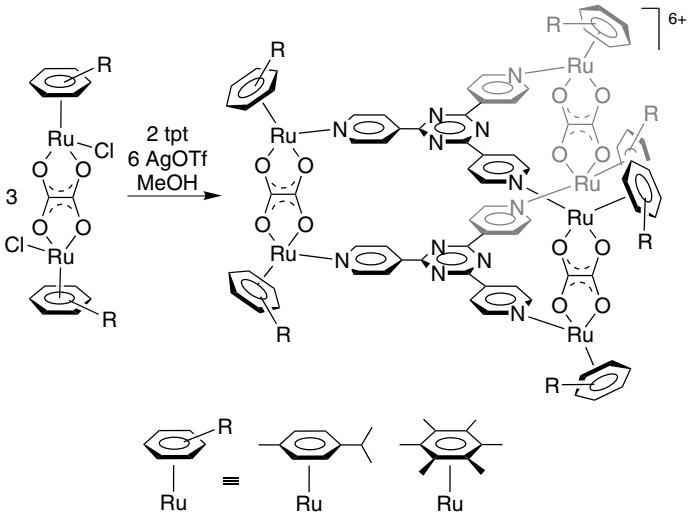

Scheme 7.8 Synthesis of trigonal prismatic cage complexes.

hexamethylbenzene complex possesses a helical chirality induced by a twist of the tpt ligands and a concerted tilt of pyridyl moieties. The helicity persists in solution as shown by NMR spectroscopic measurements.

Structurally related complexes with bridging chloro ligands instead of oxalato ligands were obtained by reaction of $[(\text{arene})\text{RuCl}(\mu\text{-Cl})]_2$ with tpt followed by abstraction of chloride by AgOTf (Figure 7.13) [57]. The metallo-prism are stabilized by π-stacking interactions between the two tpt ligands.

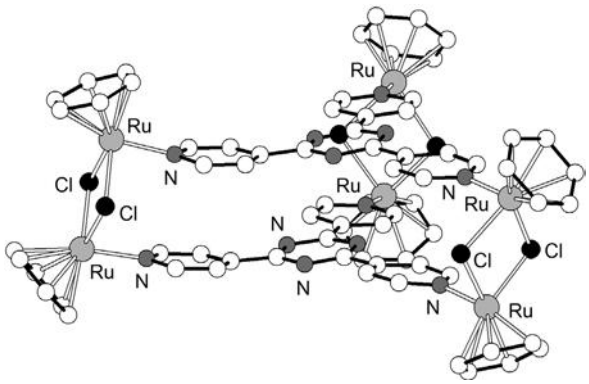

Figure 7.13 Molecular structure of the metallo-prism $[\{(p\text{-cymene})\text{Ru}\}_6(\mu_3\text{-tpt})_2(\mu\text{-Cl})_6](\text{OTf})_6$ in the crystal. The hydrogen atoms, the triflate anions and the side-chains of the π-ligands are not shown for clarity.

7.4
Expanded Helicates

Cylindrical structures with six (π-ligand)M complexes have been obtained by reaction of $[(C_6H_5Me)RuCl(\mu\text{-}Cl)]_2$ or $[(C_5Me_4H)RhCl(\mu\text{-}Cl)]_2$ with bis(dihydroxypyridine) ligands (Scheme 7.9, Figure 7.14) [58]. These hexanuclear complexes are composed of two 12-metallacrown-3 fragments, which are connected by three flexible spacers. Since the metallacrowns are chiral, the complexes can be regarded as expanded, triple-stranded helicates.

The maximum Rh-to-Rh distance of the $(C_5Me_4H)Rh$ complex shown in Figure 7.14 is 2.2 nm. The macrocycles formed between two opposite metals have a ring size of 44 atoms containing a total of 18 CH_2 groups, only eight of which are part of semi-rigid piperidine units. This complex is therefore a rare example of a discrete, multinuclear complex, which was obtained by metal-based self-assembly with a highly flexible ligand.

More detailed investigations revealed that water-soluble helicates can be obtained upon careful adjustment of the pH [59]. When 5 equiv. of CsOH were added to an aqueous solution of a mixture of $[(benzene)RuCl(\mu\text{-}Cl)]_2$ and the piperazine-bridged dihydroxypyridine ligand $[\{(C_5H_2NO_2)CH_2\}_2(C_4H_{10}N_2)](OTf)_2$ (see Scheme 7.9), a hexanuclear helicate was obtained in over 90% yield. The utilization of LiOH instead of CsOH resulted in the formation of the bis-Li^+ adduct, which displayed an even higher solubility in water. Interestingly, the latter complex is able to act as a specific receptor for the phosphate anion (Scheme 7.10). NMR titrations revealed a binding constant of 900 M^{-1} for $H_2PO_4^-$ whereas no interaction was detected for halides, nitrate and sulfate [59]. The NMR data suggest that the phosphate anion is bound in the vicinity of the bridging piperidine groups.

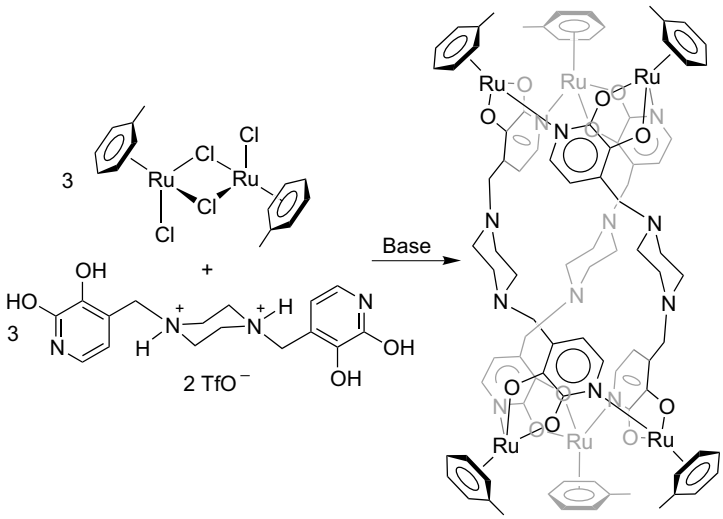

Scheme 7.9 Synthesis of an expanded helicate by base-induced assembly of (toluene)Ru complexes with bridged dihydroxypyridine ligands.

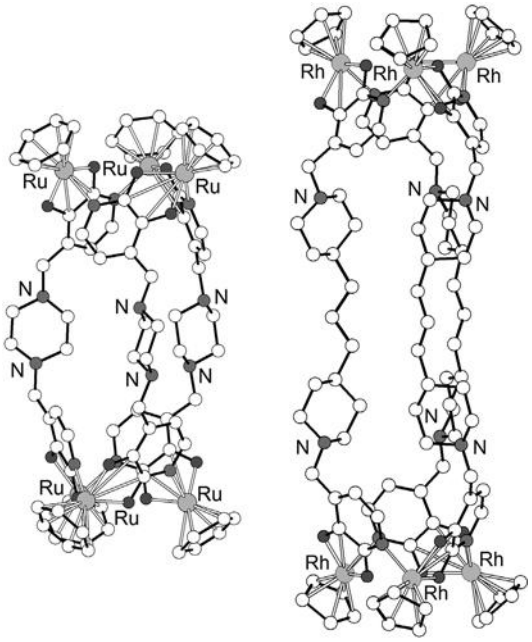

Figure 7.14 Molecular structure of two expanded helicates in the crystal. The hydrogen atoms, the solvent molecules and the side-chains of the π-ligands are not shown for clarity.

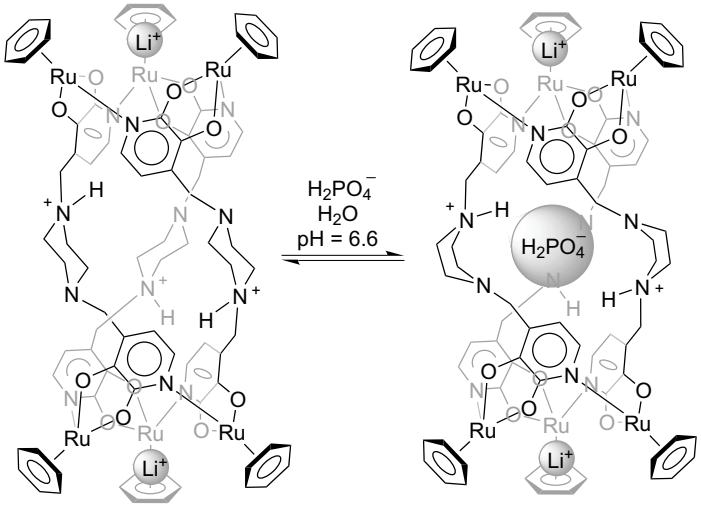

Scheme 7.10 A (benzene)Ru-based helicate is able to act as a specific receptor for the $H_2PO_4^-$ anion in aqueous solution.

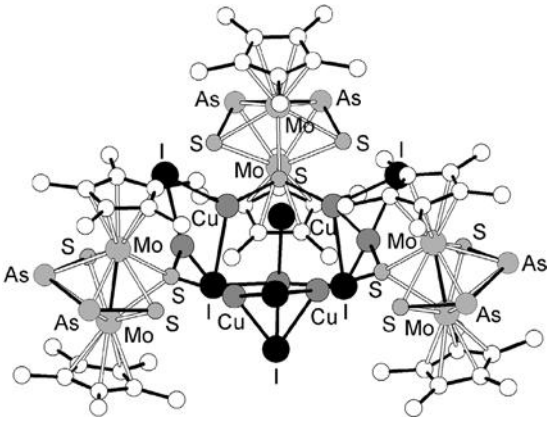

Figure 7.15 Molecular structure of $[\{(Cp^*Mo)_2As_2S_3\}_3(CuI)_7]$ in the crystal. The hydrogen atoms are not shown for clarity.

7.5 Clusters

The utility of $[Cp^*Rh]^{2+}$ in the stabilization of nanostructures was demonstrated 30 years ago for modifying the surfaces of polyoxometallate clusters. The resulting ensembles were proposed as models for oxide-supported metal catalysts. The first species of this type was $(Bu_4N)_2[Cp^*Rh(Nb_2W_4O_{19})]$, which results from the derivatization of *cis*-$[Nb_2W_4O_{19}]^{4-}$ with $[Cp^*Rh]^{2+}$ [60]. The Rh(III) center binds in a tridentate manner to $M_3(\mu_2\text{-}O)_3$ faces of the oxometallate to give all three possible diastereoisomers. In a complementary way, the species $[Cp^*Rh(OH)_2]_2$ was employed as both a ligand and as a mineralizer to depolymerize the layered binary V_2O_5. The resulting 10-vertex cluster is $[Cp^*Rh]_4(V_6O_{19})$, a derivative of the otherwise unknown anion $[V_6O_{19}]^{8-}$. Four alternating faces have been capped by the rhodium dication [61]. Half-sandwich complexes, although often derived from early metals, are valuable in developing supramolecular structures based on M−S cores. These developments are illustrated by $[(Cp^*Mo)_8Ni_8S_{16}](PF_6)_4$ [62], $Li_2(THF)_2Cp^*{}_3Ta_3S_6$ [63] and $[\{(Cp^*Mo)_2As_2S_3\}_3(CuI)_7]$ (Figure 7.15) [64].

7.6 Conclusions

Organometallic chemistry and supramolecular coordination chemistry have different roots, but the combination of these two approaches has proven powerful. The enabling advance is the exploitation of half-sandwich reagents, which are truly hemilabile – the π-ligand adheres very tightly to the metal and the other three coordination sites bind diverse ligands, ranging through hydrocarbons, amino

acids, small inorganic anions and heterocycles. The half-sandwich motif strongly suppresses polymerization reactions to a remarkable extent and the resulting molecular assemblies engage in specific host–guest interactions. It is clear that opportunities exist for further expansion of this area. Some general themes that can be expected to be particularly fruitful include nanostructures relevant to homogeneous catalysis [65], medicine [66] and sensors [67].

References

1 Shaw, B.L. (1975) *J. Am. Chem. Soc.*, **97**, 3856–3857.

2 Contakes, S.M., Klausmeyer, K.K. and Rauchfuss, T.B. (2004) *Inorg. Synth.*, **34**, 166–171.

3 Severin, K. (2006) *Chem. Commun.*, 3859–3867.

4 Boyer, J.L., Kuhlman, M.L. and Rauchfuss, T.B. (2007) *Acc. Chem. Res.*, **40**, 233–242.

5 White, C., Yates, A. and Maitlis, P.M. (1992) *Inorg. Synth.*, **29**, 228–234.

6 Zhu, B., Ellern, A., Sygula, A., Sygula, R. and Angelici, R.J. (2007) *Organometallics*, **26**, 1721–1728.

7 (a) Vecchi, P.A., Alvarez, C.M., Ellern, A., Angelici, R.J., Sygula, A., Sygula, R. and Rabideau, P.W. (2005) *Organometallics*, **24**, 4543–4552. (b) Zhu, B., Ellern, A., Sygula, A., Sygula, R. and Angelici, R.J. (2007) *Organometallics*, **26**, 1721–1728.

8 (a) Yamamoto, Y., Nakamura, H. and Ma, J.-F. (2001) *J. Organomet. Chem.*, **640**, 10–20. (b) Suzuki, H., Tajima, N., Tatsumi, K. and Yamamoto, Y. (2000) *Chem. Commun.*, 1801–1802.

9 Yamamoto, Y., Suzuki, H., Tajima, N. and Tatsumi, K. (2002) *Chem. Eur. J.*, **8**, 372–379.

10 (a) Zhang, Q.-F., Adams, R.D. and Leung, W.-H. (2006) *Inorg. Chim. Acta*, **359**, 978–983. (b) Wang, J.-Q., Ren, C.-X. and Jin, G.-X. (2006) *Organometallics*, **25**, 74–81. (c) Han, W.S. and Lee, S.W. (2004) *Dalton Trans.*, 1656–1663. (d) Yan, H., Süss-Fink, G., Neels, A. and Stoeckli-Evans, H. (1997) *J. Chem. Soc. Dalton Trans.*, 4345–4350.

11 (a) Takahata, K., Iwadate, N., Kajitani, H., Tanabe, Y. and Ishii, Y. (2007) *J. Organomet. Chem.*, **692**, 208–216. (b) Tanabe, Y., Kuwata, S. and Ishii, Y. (2002) *J. Am. Chem. Soc.*, **124**, 6528–6529.

12 Klausmeyer, K.K., Rauchfuss, T.B. and Wilson, S.R. (1998) *Angew. Chem. Int. Ed.*, **37**, 1694–1696.

13 (a) Fish, R.H. and Jaouen, G. (2003) *Organometallics*, **22**, 2166–2177. (b) Ogo, S., Buriez, O., Kerr, J.B. and Fish, R.H. (1999) *J. Organomet. Chem.*, **589**, 66–74. (c) Ogo, S., Nakamura, S., Chen, H., Isobe, K., Watanabe, Y. and Fish, R.H. (1998) *J. Org. Chem.*, **63**, 7151–7156. (d) Bakhtiar, R., Chen, H., Ogo, S. and Fish, R.H. (1997) *Chem. Commun.*, 2135–2136. (e) Chen, H., Ogo, S. and Fish, R.H. (1996) *J. Am. Chem. Soc.*, **118**, 4993–5001. (f) Chen, H., Olmstead, M.M., Smith, D. P., Maestre, M.F. and Fish, R.H. (1995) *Angew. Chem. Int. Ed. Engl.*, **34**, 1514–1517. (g) Smith, D.P., Baralt, E., Morales, B., Olmstead, M.M., Maestre, M.F. and Fish, R.H. (1992) *J. Am. Chem. Soc.*, **114**, 10647–10649.

14 Korn, S. and Sheldrick, W.S. (1997) *J. Chem. Soc. Dalton Trans.*, 2191–2199.

15 (a) Annen, P., Schildberg, S. and Sheldrick, W.S. (2000) *Inorg. Chim. Acta*, **307**, 115–124. (b) Korn, S. and Sheldrick, W.S. (1997) *Inorg. Chim. Acta*, **254**, 85–91.

16 (a) Yamanari, K., Ito, R., Yamamoto, S., Konno, T., Fuyuhiro, A., Kobayashi, M. and Arakawa, R. (2003) *Dalton Trans.*, 380–386. (b) Yamanari, K., Ito, R., Yamamoto, S. and Fuyuhiro, A. (2001) *Chem. Commun.*, 1414–1415.

17 Kunkely, H. and Vogler, A. (2002) *Inorg. Chim. Acta*, **338**, 265–267.

18 Yamanari, K., Ito, R., Yamamoto, S., Konno, T., Fuyuhiro, A., Fujioka, K. and Arakawa, R. (2002) *Inorg. Chem.*, **41**, 6824–6830.

19 Yamanari, K., Yamamoto, S., Ito, R., Kushi, Y., Fuyuhiro, A., Kubota, N., Fukuo, T. and Arakawa, R. (2001) *Angew. Chem. Int. Ed.*, **40**, 2268–2271.

20 (a) Sünkel, K., Hoffmüller, W. and Beck, W. (1998) *Z. Naturforsch., Teil B*, **53**, 1365–1368. (b) Ogo, S., Chen, H., Olmstead, M.M. and Fish, R.H. (1996) *Organometallics*, **15**, 2009–2013. (c) Krämer, R., Polborn, K., Robl, C. and Beck, W. (1992) *Inorg. Chim. Acta*, **198–200**, 415–420.

21 (a) Carmona, D., Lamata, M.P., Viguri, F., Dobrinovich, I., Lahoz, F.J. and Oro, L.A. (2002) *Adv. Synth. Catal.*, **344**, 499–502. (b) Kathó, Á., Carmona, D., Viguri, F., Remacha, C.D., Kovács, J., Joó, F. and Oro, L.A. (2000) *J. Organomet. Chem.*, **593–594**, 299–306. (c) Carmona, D., Lahoz, F.J., Atencio, R., Oro, L.A., Lamata, M.P., Viguri, F., José, E.S., Vega, C., Reyes, J., Joó, F. and Kathó, Á. (1999) *Chem. Eur. J.*, **5**, 1544–1564.

22 Piotrowski, H., Polborn, K., Hilt, G. and Severin, K. (2001) *J. Am. Chem. Soc.*, **123**, 2699–2700.

23 Piotrowski, H., Hilt, G., Schulz, A., Mayer, P., Polborn, K. and Severin, K. (2001) *Chem. Eur. J.*, **7**, 3196–3208.

24 Lehaire, M.-L., Scopelliti, R., Herdeis, L., Polborn, K., Mayer, P. and Severin, K. (2004) *Inorg. Chem.*, **43**, 1609–1617.

25 Habereder, T., Warchhold, M., Nöth, H. and Severin, K. (1999) *Angew. Chem. Int. Ed.*, **38**, 3225–3228.

26 (a) Missami, L., Cordier, C., Guyard-Duhayon, C., Mann, B.E. and Amori, H. (2007) *Organometallics*, **26**, 860–864. (b) Missami, L., Guyard-Duhayon, C., Rager, M.N. and Amouri, H. (2004) *Inorg. Chem.*, **43**, 6644–6649.

27 For a review on metallacrown complexes, see Mezei, G., Zaleski, C.M. and Pecoraro, V.L. (2007) *Chem. Rev.*, **107**, 4933–5003.

28 Lehaire, M.-L., Schulz, A., Scopelliti, R. and Severin, K. (2003) *Inorg. Chem.*, **42**, 3576–3581.

29 (a) Lehaire, M.-L., Scopelliti, R., Piotrowski, H. and Severin, K. (2002) *Angew. Chem. Int. Ed.*, **41**, 1419–1422. (b) Lehaire, M.-L., Scopelliti, R. and Severin, K. (2002) *Inorg. Chem.*, **41**, 5466–5474.

30 Lehaire, M.-L., Scopelliti, R. and Severin, K. (2002) *Chem Commun.*, 2766–2767.

31 Grote, Z., Wizemann, H.-D., Scopelliti, R. and Severin, K. (2007) *Z. Anorg. Allg. Chem.*, **633**, 858–864.

32 Piotrowski, H. and Severin, K. (2002) *Proc. Natl. Acad. Sci. USA*, **99**, 4997–5000.

33 (a) Pilcher, H.R. (2003) *Nature*, **425**, 118–120. (b) Birch, N.J. (1999) *Chem. Rev.*, **99**, 2659–2682. (c) Bartsch, R.A., Ramesh, V., Bach, R.O., Shono, T. and Kimura, K. (1995) in *Lithium Chemistry*, (eds A.-M. Sapse and P.v.R. Schleyer),Wiley, New York, pp. 393–476.

34 (a) Grote, Z., Scopelliti, R. and Severin, K. (2004) *J. Am. Chem. Soc.*, **126**, 16959–16972. (b) Grote, Z., Lehaire, M.-L., Scopelliti, R. and Severin, K. (2003) *J. Am. Chem. Soc.*, **125**, 13638–13639.

35 Corbett, P.T., Leclaire, J., Vial, L., West, K. R., Wietor, J.-L., Sanders, J.K.M. and Otto, S. (2006) *Chem. Rev.*, **106**, 3652–3711.

36 (a) Grote, Z., Scopelliti, R. and Severin, K. (2007) *Eur. J. Inorg. Chem.*, 694–700. (b) Saur, I., Scopelliti, R. and Severin, K. (2006) *Chem. Eur. J.*, **12**, 1058–1066. (c) Saur, I. and Severin, K. (2005) *Chem. Commun.*, 1471–1473. (d) Grote, Z., Scopelliti, R. and Severin, K. (2003) *Angew. Chem. Int. Ed.*, **42**, 3821–3825.

37 Amouri, H., Rager, M.N., Cagnol, F. and Vaissermann, J. (2001) *Angew. Chem. Int. Ed.*, **40**, 3636–3638.

38 Dunbar, K.R. and Heintz, R.A. (1997) *Prog. Inorg. Chem.*, **45**, 283–391.

39 Evans, R.F., Ormrod, O., Goalby, B.B. and Staveley, L.A.K. (1950) *J. Chem. Soc.*, 3346.

40 (a) Boxhoorn, G., Moolhuysen, J., Coolegem, J.G.F. and van Santen, R.A. (1985) *J. Chem. Soc., Chem. Commun.*, 1305–1306. (b) Chapman, K.W., Southon,

P.D., Weeks, C.L. and Kepert, C.J. (2005) *Chem. Commun.*, 3322–3324. (c) Kaye, S.S. and Long, J.R. (2005) *J. Am. Chem. Soc.*, **127**, 6506–6507. (d) Ramprasad, D., Markley, T.J. and Pez, G.P. (1997) *J. Mol. Catal. A*, **117**, 273–278. (e) Meier, I.K., Pearlstein, R.M., Ramprasad, D. and Pez, G.P. (1997) *Inorg. Chem.*, **36**, 1707–1714. (f) Ramprasad, D., Pez, G.P., Toby, B.H., Markley, T.J. and Pearlstein, R. M. (1995) *J. Am. Chem. Soc.*, **117**, 10694–10701.

41 Prout, W.E., Russell, E.R. and Groh, H.J. (1965) *J. Inorg. Nucl. Chem.*, **27**, 473–479.

42 Klausmeyer, K.K., Rauchfuss, T.B. and Wilson, S.R. (1998) *Angew. Chem. Int. Ed.*, **37**, 1694–1696.

43 Contakes, S.M., Kuhlman, M.L., Ramesh, M., Wilson, S.R. and Rauchfuss, T.B. (2002) *Proc. Natl. Acad. Sci. U.S.A.*, **99**, 4889–4893.

44 Bryan, J.C., Kavallieratos, K. and Sachleben, R.A. (2000) *Inorg. Chem.*, **39**, 1568–1572.

45 Hsu, S.C.N., Ramesh, M., Espenson, J.H. and Rauchfuss, T.B. (2003) *Angew. Chem. Int. Ed.*, **42**, 2663–2666.

46 (a) Contakes, S.M. and Rauchfuss, T.B. (2000) *Angew. Chem. Int. Ed.*, **39**, 1984–1986. (b) Contakes, S.M. and Rauchfuss, T.B. (2001) *Chem. Commun.*, 553–554.

47 Boyer, J.L., Ramesh, M., Yao, H., Rauchfuss, T.B. and Wilson, S.R. (2007) *J. Am. Chem. Soc.*, **129**, 1931–1936.

48 Contakes, S.M., Klausmeyer, K.K., Milberg, R.M., Wilson, S.R. and Rauchfuss, T.B. (1998) *Organometallics*, **17**, 3633–3635.

49 Boyer, J.L., Yao, H., Kuhlman, M.L., Rauchfuss, T.B. and Wilson, S.R. (2007) *Eur. J. Inorg. Chem.*, 2721–2728.

50 Kuhlman, M.L. and Rauchfuss, T.B. (2003) *J. Am. Chem. Soc.*, **125**, 10084–10092.

51 Beltran, L.M.C. and Long, J.R. (2005) *Acc. Chem. Res.*, **38**, 325–334.

52 Lang, J.-P., Xu, Q.-F., Chen, Z.-N. and Abrahams, B.F. (2003) *J. Am. Chem. Soc.*, **125**, 12682–12683.

53 Kuhlman, M.L., Yao, H. and Rauchfuss, T.B. (2004) *Chem. Commun.*, 1370–1371.

54 Brasey, T., Scopelliti, R. and Severin, K. (2006) *Chem. Commun.*, 3308–3310.

55 Mirtschin, S., Krasniqi, E., Scopelliti, R. and Severin, K. in preparation.

56 Govindaswamy, P., Linder, D., Lacour, J., Süss-Fink, G. and Therrien, B. (2006) *Chem. Commun.*, 4691–4693.

57 Govindaswamy, P., Süss-Fink, G. and Therrien, B. (2007) *Organometallics*, **26**, 915–924.

58 Grote, Z., Bonazzi, S., Scopelliti, R. and Severin, K. (2006) *J. Am. Chem. Soc.*, **128**, 10382–10383.

59 Olivier, C., Grote, Z., Solari, E., Scopelliti, R. and Severin, K. (2007) *Chem. Commun.*, 4000–4002.

60 Besecker, C.J., Day, V.W., Klemperer, W.G. and Thompson, M.R. (1984) *J. Am. Chem. Soc.*, **106**, 4125–4136.

61 (a) Chae, H.K., Klemperer, W.G. and Day, V.W. (1989) *Inorg. Chem.*, **28**, 1423–1424. (b) Chae, H.K., Klemperer, W.G., Paez-Loyo, D.E., Day, V.W. and Eberspacher, T. A. (1992) *Inorg. Chem.*, **31**, 3187–3189.

62 Takei, I., Suzuki, K., Enta, Y., Dohki, K., Suzuki, T., Mizobe, Y. and Hidai, M. (2003) *Organometallics*, **22**, 1790–1792.

63 Tatsumi, K., Inoue, Y., Kawaguchi, H., Kohsaka, M., Nakamura, A., Cramer, R.E., VanDoorne, W., Taogoshi, G.J. and Richmann, P.N. (1993) *Organometallics*, **12**, 352–364.

64 Pronold, M., Scheer, M., Wachter, J. and Zabel, M. (2007) *Inorg. Chem.*, **46**, 1396–1400.

65 (a) Fiedler, D., Leung, D.H., Bergman, R. G. and Raymond, K.N. (2005) *Acc. Chem. Res.*, **38**, 349–358. (b) Thomas, C.M. and Ward, T.R. (2005) *Chem. Soc. Rev.*, **34**, 337–346.

66 (a) Allardyce, C.A. and Dyson, P. (2006) *Top. Organomet. Chem.*, **17**, 177–210. (b) G. Jaouen, (ed.) (2005) *Bioorganometallics*, Wiley-VCH, Weinheim.

67 Severin, K. (2006) *Top. Organomet. Chem.*, **17**, 123–142.

8
Endochemistry of Self-assembled Hollow Spherical Cages

Takashi Murase and Makoto Fujita

8.1
Introduction

Nature has developed a variety of macromolecules with high catalytic efficiency and extraordinary versatility in reactions whose rates can be accelerated. Such chemical reactions take place in well-defined and confined environments, which vary from nanometer-sized and relatively simple systems, such as enzymes, to micrometer-sized and extremely complex assemblies, such as cells [1a]. In this context, chemistry inside a cage-like architecture (endohedral chemistry, "endochemistry") prevails everywhere in biological systems (Figure 8.1). The specificity and precision displayed by biological systems are derived from the highly directed mutual recognition process displayed by the components of a structure, so-called "self-assembly" [1b]. Self-assembly of molecules is a ubiquitous strategy to create functional assemblages in nature. Recent developments in noncovalent synthesis employing self-assembly of multiple constituent molecules have made it possible to prepare readily large and hollow cage architectures, which can hardly be obtained otherwise by conventional covalent methods [1]. However, in molecular nanotechnology, the technique of molecular self-assembly is not yet fully exploited for the functionalization of interior surfaces of hollow cage compounds.

To date, a self-assembled spherical cage compound can be roughly classified into two categories: (1) *biomacromolecular cages*, which have various sizes and can be redesigned by altering their chemical composition to attain a desired structure and function, and (2) *polymer micelles*, self-assembled from multi-block copolymers, which consist of hydrophilic and hydrophobic chain segments with pre- or post-attached functionalities [2]. The above spherical compounds are truly prominent and fascinating materials/scaffolds for endohedral functionalization of a restricted nanosized region and have been summarized elsewhere. In this chapter, we will briefly describe the aspects of endohedral functionalization of these existing cage compounds and then focus on the latest findings from our own laboratory.

Organic Nanostructures. Edited by Jerry L. Atwood and Jonathan W. Steed

ISBN: 978-3-527-31836-0

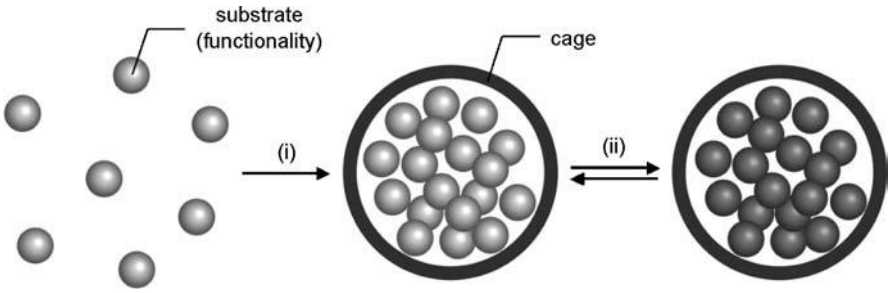

Figure 8.1 Schematic image of endochemistry in a confined region: (i) concentration of substrate/functionality (ii) chemical reaction and dynamic change.

8.2 Biomacromolecular Cages

Biomimetic chemistry offers a new approach to synthesize nanomaterials [3]. Protein cages and viral protein cages (capsides) share the common characteristics of self-assembly from a specific set of subunits into well-defined and highly symmetrical architectures. One example is an iron-storage protein, ferritin [4a]. Iron-free ferritin molecules (apo-ferritin) are composed of 24 polypeptide subunits, which self-assemble into a hollow spherical cage with a molecular mass of 450 kDa. Ferritin has an outer diameter of 12 nm and an inner cavity diameter of 8 nm that stores iron in the form of microcrystalline ferric oxyhydroxide [4b]. Another example is Cowpea Chlorotic Mottle Virus (CCMV) capside, which is composed of 180 identical 20-kDa subunits and has an outer diameter of 28 nm and an inner diameter ranging from 18 to 24 nm [5]. These organized biomacromolecular architectures can serve as not only nanoreactors or nanotemplates for crystallizations and other reactions, but also spatially defined scaffolds for the attachment of new chemical functionalities. Therefore, they possess the potential to be used to express and adjust multivalent presentations [6]. When functional groups are confined in these biomolecular cages by interior modification, the number and position of the functional groups are precisely controlled. So far, interior modification has lagged behind exterior modification, but intriguing and sophisticated studies have already been conducted [7].

However, the cavities of these protein cages, especially capsides, are too large to place functional groups at the cores. The types of functionalities introduced by genetic modification are limited to amino acids that mainly serve as "reactive sites" on the interior surfaces of cages. Chemical modification is mainly conducted to the already self-assembled spherical cages, which demands excess reagents to attach functionalities at all reactive sites, resulting in a poor introduction efficiency. Therefore, the current usage of the cavities of the protein cages remains as nanotemplates for inorganic materials.

8.3
Polymer Micelles

Polymer micelles are formed spontaneously by amphiphilic block copolymers in aqueous solution. By tailoring the relative lengths between the hydrophobic and hydrophilic blocks, compositions and self-assembly conditions, micellar aggregates with various morphologies (including star micelles, crew-cut micelles, rods and vesicles) can be designed and synthesized [8]. The spherical polymer micelle possesses a unique core–shell structure, which can be modified both chemically and structurally by the introduction of functionality at particular positions within the nanoarchitecture. In a typical spherical core–shell diblock polymer micelle, the introduction of functionality at the hydrophilic and hydrophobic chain blocks corresponds to the surface/shell and core functionalization, respectively [9].

The endohedral core functionalization of polymer micelles has attracted much interest, due to their potential applications, such as drug delivery carriers or nanoreactors. However, compared with the surface/shell functionalization, the functionalization of the core domain within polymer micelles has received limited attention, perhaps because of the difficulty in introducing and maintaining functionality within the hydrophobic block [9]. The functional groups in the hydrophobic block are supposed to be closely packed and concentrated at the core domain in the self-assembly process. Therefore, not only the hydrophobic properties but also the molecular sizes of the functional groups seem to affect greatly the formation of polymer micelles. Some notable studies on core functionalization of polymer micelles have been reported [10]. However, as a whole, endohedral functionalization of polymer micelles is regarded as a difficult but challenging task. A significant difference between polymer micelles and biomacromolecules is that in polymer micelles it is impossible to control precisely the number and position of the introduced functional groups. The molecular weight of the polymer micelles is not monodispersive and hydrophobic interaction under the self-assembly process does not have an orientation with a clear direction. Therefore, in the true sense, the polymer micelles do not have well-defined structures and shapes.

8.4
$M_{12}L_{24}$ Spheres

8.4.1
Self-assembly of $M_{12}L_{24}$ Spheres

To control precisely the number and position of functional groups introduced in a confined region, it is necessary to develop a novel nanosized cage compound having a well-defined chemical structure and an inner diameter that is suitable to confine the functional groups. Moreover, the introduction of functionality should be carried out in the subunit level before the self-assembly process, where the desired functionality is attached appropriately and efficiently to each component. However, to date, it has

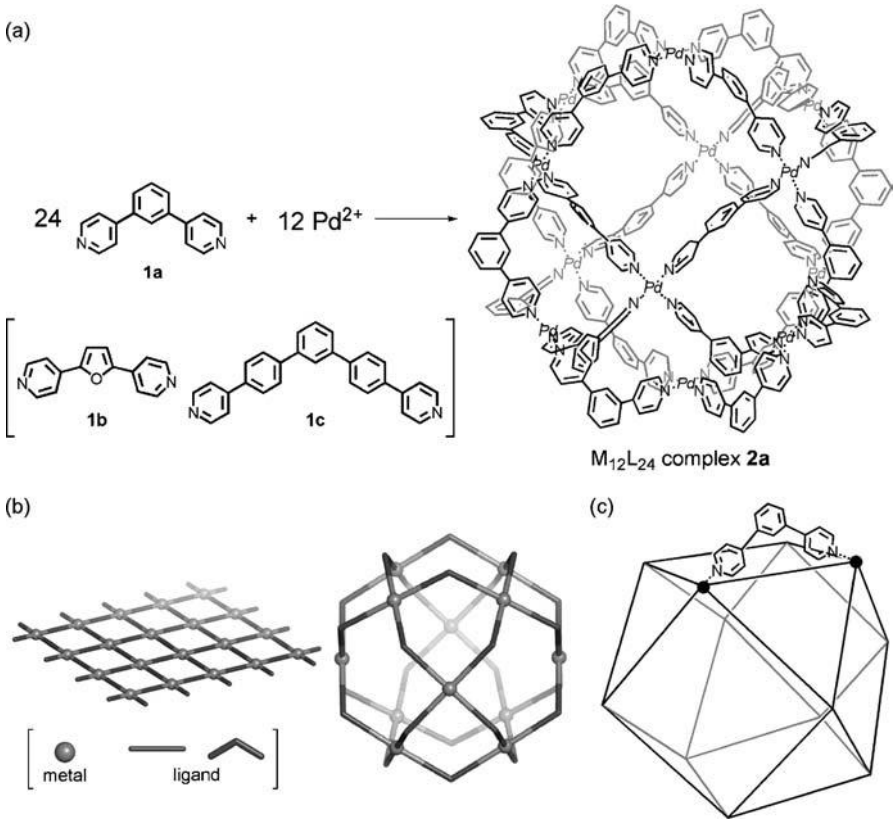

Figure 8.2 (a) Self-assembly of an $M_{12}L_{24}$ spherical complex. (b) Linear ligand (2D grid infinite network) vs. bent ligand (spherical finite complex). (c) Schematic representation of the cubo-octahedral frameworks of **2a** [11].

been difficult to synthesize artificially virus-like huge but well-defined spherical hollow cages.

In 2004, we demonstrated that a spherical coordination network, $M_{12}L_{24}$, can be prepared in a quantitative yield from 36 components, i.e. 12 metal ions (M) and 24 bridging ligands (L) (Figure 8.2a) [11]. The complexation of the bent bidentate ligands with naked square-planar palladium(II) ions affords a discrete spherical complex, in contrast to the 2D infinite network formation from linear ligands (Figure 8.2b). The symmetry of self-assembled $M_{12}L_{24}$ spherical complexes is depicted by a cuboctahedron, which is formed by truncating each of the eight vertices of a cube to produce eight triangular faces (Figure 8.2c). The 12 equivalent vertices and 24 equivalent edges of the cuboctahedron can be superimposed on the 12 palladium(II) centers and 24 bridging ligands, respectively. Such a highly symmetrical and huge structure has been unambiguously confirmed by X-ray crystallographic analysis of spherical

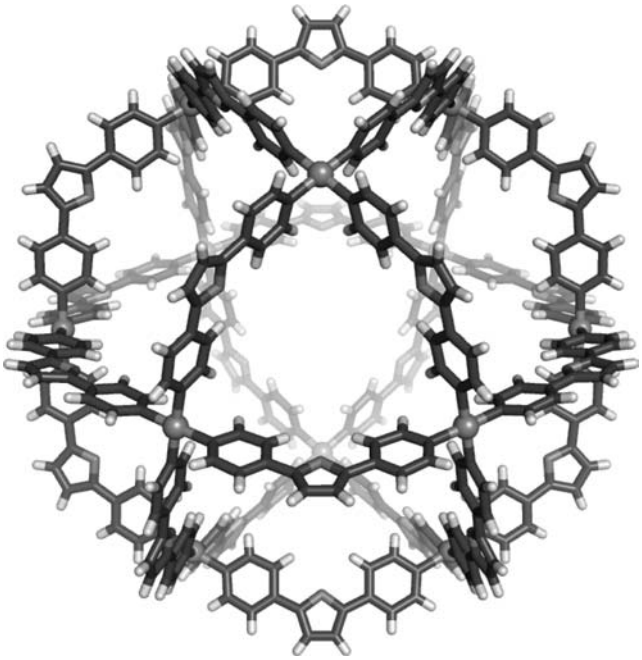

Figure 8.3 X-ray crystal structure of $M_{12}L_{24}$ spherical complex **2b**.

complex **2b**, which is an analogue of **2a** where the bending center of the ligand, *m*-phenylene, is replaced with 2,5-furanylene (Figure 8.3).

8.4.2
Endohedral Functionalization of $M_{12}L_{24}$ Spheres

The surface functionalization of $M_{12}L_{24}$ spherical complexes is readily conducted by attaching a functional group on the convex side of ligand **1a**, resulting in the equivalent alignment of 24 functional groups at the periphery of the spherical complex. It has been demonstrated that large functional groups, such as fullerene [11], porphyrin [11] and oligosaccharide [12], can be introduced on the surface of spherical complex **2a**.

It was expected that if a functional group was attached to the concave side of the ligand **1a**, the endohedral functionalization of the $M_{12}L_{24}$ spherical complex would be accomplished. However, ligand **1a**, having a methyl group at the concave side (ligand **1d**), did not assemble into the $M_{12}L_{24}$ complex upon complexation with Pd(II) ions [13]. It is considered that the steric repulsion between the pyridyl groups and the attached methyl group causes a nonplanar conformation of the ligand and that such a twisted conformation is not favorable for the complexation (Figure 8.4a). The drawback was removed by inserting an acetylene spacer between the pyridine coordination sites and the core benzene ring to expand the cavity of the complex (ligand **1e**) (Figure 8.4b). Hence the above result indicates that, at each Pd(II) center of

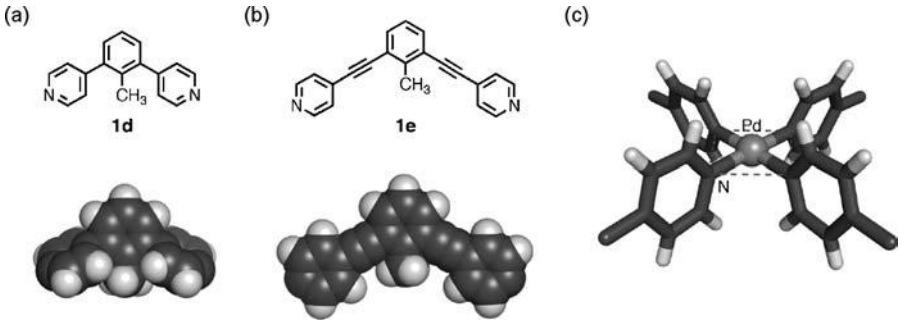

Figure 8.4 Molecular modeling of (a) **1d** and (b) **1e** optimized by a force-field calculation. (c) Partial structure around the Pd coordination center.

the $M_{12}L_{24}$ complex, a perpendicular array of four pyridyl groups with respect to the PdN_4 plane should be essential to the self-assembly of the spherical complex (Figure 8.4c). The acetylene-mediated $M_{12}L_{24}$ spherical complex has an outer diameter of 4.6 nm and an inner diameter of approximately 3.7 nm and serves as a versatile scaffold for endohedral functionalization, as shown schematically in Figure 8.5 [13].

8.4.3
Fluorous Nanodroplets

The term "fluorous" was introduced as an analogy to "aqueous" or "aqueous media" for highly fluorinated alkanes, ethers and tertiary amines [14]. Fluorous solvents do not mix with most common organic solvents at room temperature. Therefore, fluorous molecules have been widely used to separate products and catalysts or products and reagents, purify mixtures and control reactions [14,15]. The creation of a

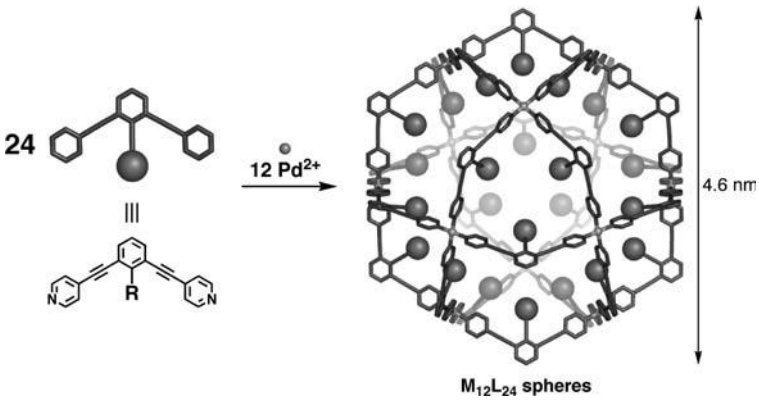

Figure 8.5 Schematic image of a self-assembled $M_{12}L_{24}$ spherical complex with 24 endohedral functional groups [13].

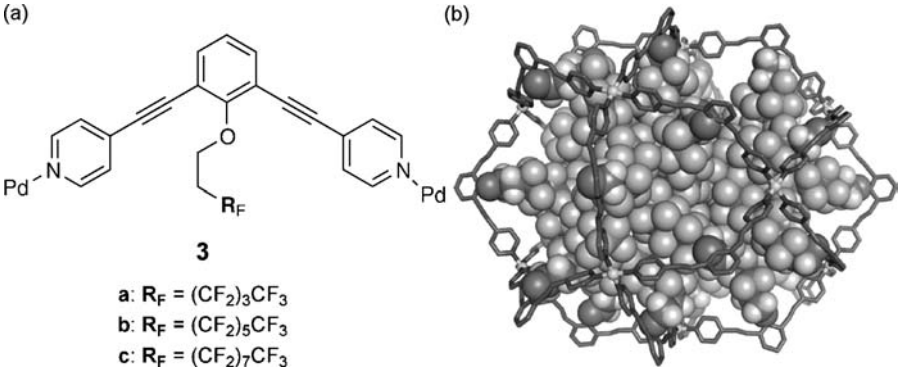

Figure 8.6 (a) $M_{12}L_{24}$ spheres **3a**–**c** with 24 perfluoroalkyl chains [17]. (b) Molecular drawing prepared by combining the X-ray crystal structure of the shell framework and the optimized $C_6F_{13}(CH_2)_2$– side-chains. The side-chains are shown as CPK representation.

fluorous microenvironment within organic cage compounds, such as vesicles, micelles and dendrimers, has already been demonstrated by some groups [16]. However, the fluorous phases are not distinctly determined physically and structurally.

A distinct endofluorous environment is created in an $M_{12}L_{24}$ spherical cage where 24 perfluoroalkyl chains reside (Figure 8.6a) [17]. $M_{12}L_{24}$ spheres have sufficiently large cavities and the perfluoroalkyl C_6F_{13} chains of complex **3b**, for example, do not completely fill the sphere, leaving a void space at the core. The fluorous core of sphere **3b** can extract an average of 5.8 molecules of perfluorooctane **4** from the suspension in DMSO solution. Detailed analysis of ^{19}F NMR spectra showed that the incorporated guest molecules were accumulated at the core of the spherical hollow complex and surrounded by the terminal portions of the perfluoroalkyl chains. The crystallographic analysis of the sphere **3b** containing the guest **4** revealed that the rigid shell framework and amorphous interior, just like a "raw egg" (Figure 8.6b). This observation indicates that the fluorinated segments furnish a fluid-like or "nanodroplet" environment. The shell framework in the crystalline state was not spherical but oval with dimensions of 4.9 nm by 4.2 nm probably because of the aggregation of the fluorous chains in the shell. Perfluorooctane is miscible in CH_3CN. Therefore, the guest molecules can be re-extracted from the core of sphere **3b** by addition of CH_3CN to the solution. The reversible uptake of fluorous compounds assures that the sphere **3b** can be recycled as a nanosized fluorous medium.

The ability to dissolve perfluoroalkanes in the endofluorous phase largely depends on the lengths of the attached perfluoroalkyl tails (Figure 8.7). Sphere **3c** with longer perfluoroalkyl tails should have a less effective void volume at the core. Therefore, the sphere **3c** can accommodate a smaller amount of perfluorooctane (ca. 2.5 guest molecules per sphere **3c**). In contrast, sphere **3a** with shorter perfluoroalkyl tails has too large a void space to confine perfluorooctane, because of insufficient fluorine

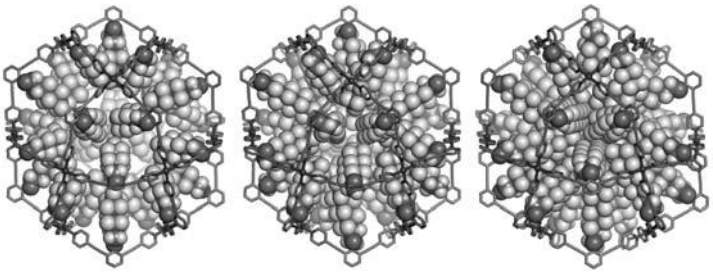

sphere	3a	3b	3c
the number of accommodated guest **4**	none	5.8	2.5

Figure 8.7 The number of accommodated guest **4** in endofluorous spheres **3a**–**c**.

density to define the fluorous atmosphere. The amount of the encapsulated guests in the spheres also depends on the molecular sizes of the guests. For example, a smaller size of a fluorocarbon guest, perfluorohexane, can be extracted in larger amounts by sphere **3b** (ca. 8.6 guest molecules per sphere **3b**). The endofluorous spheres offer a finely tunable environment for fluorous chemistry.

8.4.4
Uptake of Metal Ions into a Cage

Pyridine is a well-known monodentate ligand that can interact with a variety of metal ions. However, pyridine and pyridine-related ligands are not used as functional groups attached to a ligand of an $M_{12}L_{24}$ sphere because such functional groups bind to a Pd(II) ion and inhibit the formation of the sphere. Therefore, to encapsulate metal ions in an $M_{12}L_{24}$ cage, it is necessary to choose a functional group that has the properties to bind strongly to metal ions other than a Pd(II) ion and not to prevent the formation of the $M_{12}L_{24}$ shell structure. This requirement can be satisfied by considering that a Pd(II) ion is a soft acid in Pearson's hard and soft acids and bases (HSAB) theory [18].

When an oligo(ethylene oxide) chain is attached to each ligand, the $M_{12}L_{24}$ sphere **5** is obtained quantitatively (Figure 8.8) [13]. The cavity of complex **5** is filled with a "pseudo-nanoparticle" of poly(ethylene oxide) whose 120 ($=5\times24$) ether oxygen donors (hard bases) in total can bind rare earth and alkaline earth metal ions (hard acids) (Figure 8.9). The ^{1}H NMR spectrum of the acetonitrile solution of complex **5** and $La(OTf)_3$ revealed that the signals of ethylene oxide chain, especially terminal $-OCH_3$, were shifted downfield, whereas the signals of the aromatic shell of complex **5** remained almost unchanged. These results indicates that La(III) ions are absorbed into the poly(ethylene oxide) core to form La(III)–ethylene oxide complexes inside the complex **5**. The complexation ratio of La(III) ion to each $(OCH_2CH_2)_4OCH_3$ chain

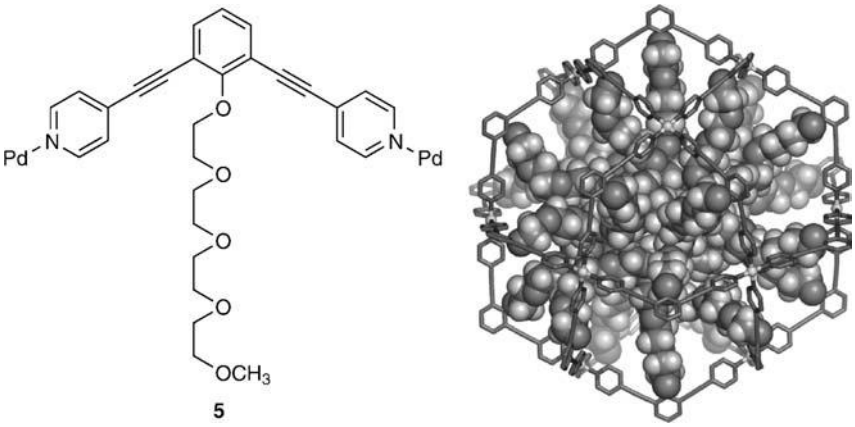

Figure 8.8 Molecular modeling of $M_{12}L_{24}$ sphere **5** with 24 oligo (ethylene oxide) chains. Side-chains are shown as CPK representation [13].

was estimated to be roughly 1:1 from the Job's plot. Thus complex **5** can take up to ca. 20 La(III) ions within the sphere. The incorporated metal ions are completely expelled from the cavity by adding 5 vol.% dimethyl sulfoxide (which strongly solvates many kinds of metal cations). The reversible uptake of metal ions can be accomplished by precisely designing a coordinative functional group and selecting solvents.

8.4.5
Polymerization in a Nutshell

Polymerization in a closed shell gives size- and/or conformation-restricted products. If such a polymerization proceeds in a nanosized region without any volumetric shrinkage, the physical and optical properties of the polymerized region will change dramatically with nanoscale resolution. Therefore, endohedral polymerization in a restricted nanosized region is an important technique to develop the high-density

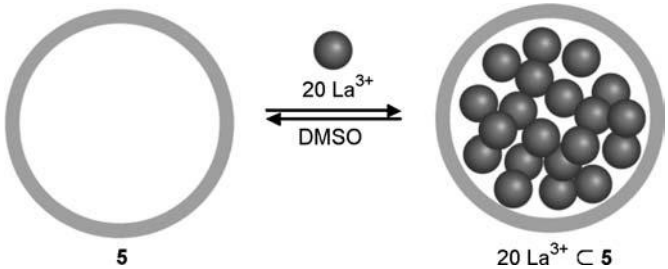

Figure 8.9 Schematic image of the reversible uptake of La(III) ions into sphere **5**.

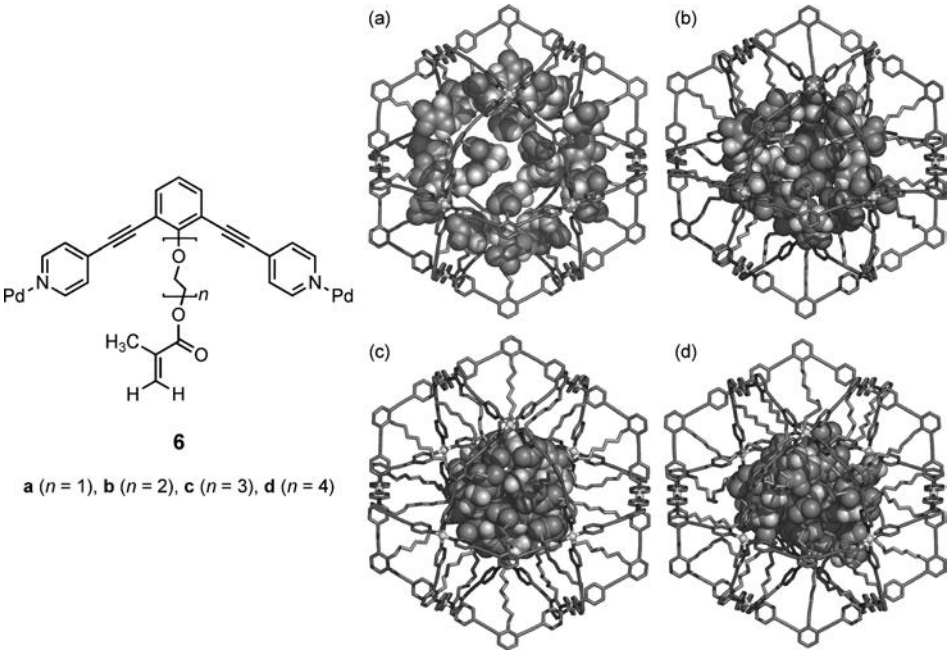

Figure 8.10 Molecular modeling of $M_{12}L_{24}$ spheres **6a–d** with 24 MMA units: (a) **6a**; (b) **6b**; (c) **6c**; (d) **6d**. MMA units are shown as CPK representation [22].

data-storage materials of the next generation [19]. Well-defined nanosized spaces or channels have been exploited to promote polymerization, including zeolites [20], porous organic crystals [20] and porous coordination polymers [21]. However, none of these host materials are discrete and it is impossible to handle them as "molecular-sized" nanoparticles.

When a polymerizable functional group, methyl methacrylate (MMA), is attached to the terminal end of each ligand via an oligo(ethylene oxide) linker, 24 MMA units are confined within molecular spheres **6a–d** (Figure 8.10) [22]. Molecular modeling of spheres **6a–d** illustrates that the relative position of MMA units in the spheres can be precisely controlled by tuning the linker length. Radical polymerization in the spherical shell **6c** proceeds in DMSO solution at 70°C using 2,2′-azobis(isobutyronitrile) (AIBN) as radical initiator. After the polymerization for 17 h, 73% of the MMA units can be converted into PMMA oligomers (Figure 8.11). The MMA monomers tethered to the shell are not completely fluid. A radical center at the end of the growing polymer should be hardly accessible to unreacted MMA monomers far from the radical. Therefore, the value of approximately 70% conversion is the maximum value of the endohedral polymerization in the shell. The aromatic shell structure is maintained during the polymerization. Diffusion-ordered NMR spectroscopy (DOSY) data support the view that the polymerization proceeds only in

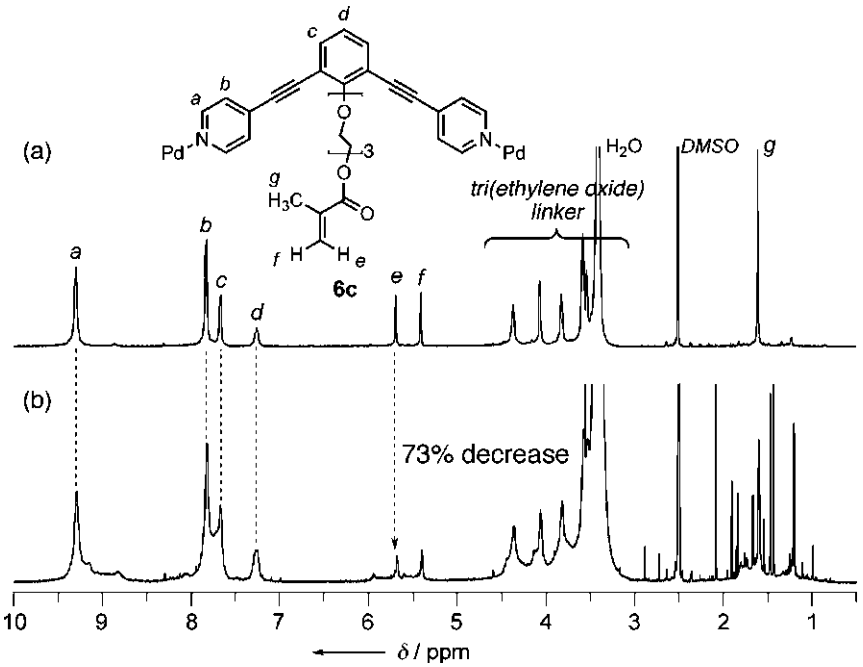

Figure 8.11 ^{1}H NMR spectra of complex **6c** (a) before and (b) after polymerization (500 MHz, DMSO-d_6, 300 K, TMS) [22].

the shell because the diffusion coefficient of the complex **6c** did not change before and after the polymerization. For application to memory storage materials, neither stereoregulation nor molecular weight control is particularly important, but polymerization only in a nanoscopically restricted region is very important. In this context, the polymerizable sphere **6c** is a highly promising material for such an application. The practical concentration of MMA units in the sphere **6c** becomes as high as 1.5 M. Therefore, even at very low concentrations of monomer, the monomers tethered to the shell are concentrated and efficiently polymerized in the sphere.

The length of the oligo(ethylene oxide) linker is extremely important in the endohedral polymerization of spheres. The tri(ethylene oxide) linker affords the best efficiency (73% conversion), because the 24 MMA units are the most closely packed at the core of the sphere **6c**. The mono- and di(ethylene oxide) linkers are too short for polymerization in the sphere, preventing the frequent close approach of MMA units (22 and 29% conversion, respectively). Meanwhile, the tetra(ethylene oxide) linker is slightly too long, resulting in the repulsion of the monomer units at the core (62% conversion). The length of the oligo(ethylene oxide) linker is adjustable to other reactive monomer units with different molecular sizes. Therefore, the present method is widely applicable to the preparation of a variety of endo-reactive molecular spheres.

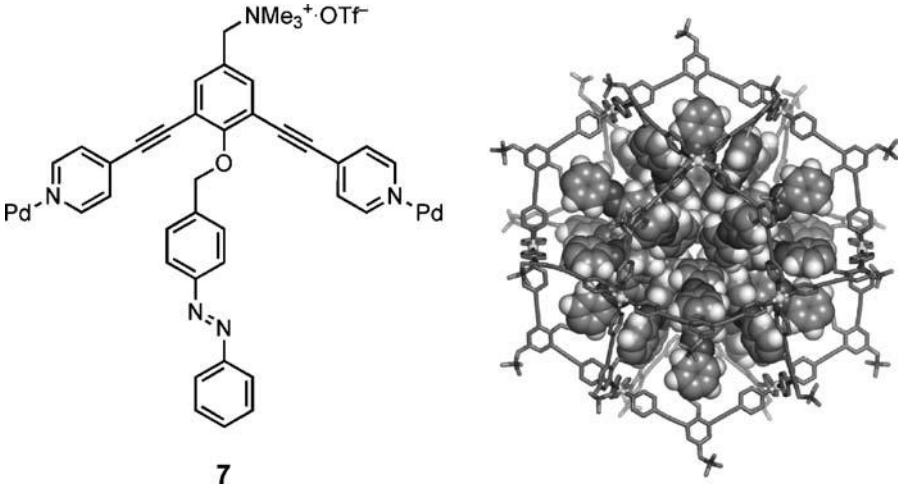

7

Figure 8.12 Molecular modeling of $M_{12}L_{24}$ sphere **7** with 24 azobenzene chromophores [25]. Azobenzene moieties are shown as CPK representation.

8.4.6
Photoresponsive Molecular Nanoballs

Azobenzene is a well-known chromophore that responds to light and undergoes *cis–trans* isomerization, resulting in large changes in its size and polarity [23]. Azobenzene-containing copolymers and dendrimers are promising photoresponsive materials and the changes of their local structures and properties have attracted a great deal of attention [24]. However, it is synthetically troublesome to confine a restricted number of azobenzene chromophores in their core regions.

Azobenzene-containing $M_{12}L_{24}$ sphere **7** is readily and quantitatively obtained from the corresponding ligand (Figure 8.12) [25]. The quaternary ammonium cations of the surface of the sphere are useful to enhance the water durability. Not all the *trans*-azobenzenes in sphere **7** can be converted to the *cis*-azobenzenes upon UV irradiation. The absorption of UV light by the shell structure is supposed to suppress the *trans–cis* isomerization to be ca. 20% conversion at the photostationary state. Thermally unstable *cis*-azobenzene moieties in sphere **7** are completely returned to the initial *trans* forms by heating at 50°C.

The sphere **7** can accommodate ca. 16–20 molecules of pyrene in a $CH_3CN–H_2O$ mixed solvent. Neither free ligand nor empty sphere can exert such an effect. Therefore, hydrophobic accumulation of *trans*-azobenzene moieties in the sphere is essential to the guest uptake. Molecular modeling of sphere **7** suggests that the assembled 24 azobenzene moieties construct triangular and square cavities in the sphere, which serve as hydrophobic pockets or portals. The encapsulated pyrenes are magnetically shielded in the sphere and the degree of shielding increases with

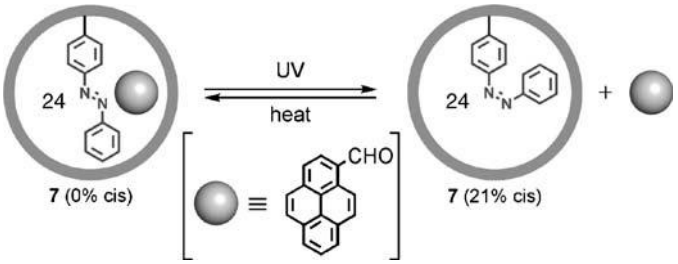

Figure 8.13 Reversible uptake of hydrophobic guests into sphere **7** by alternatively applying UV light and heat.

increase in the ratio of H_2O. These results support the existence of host–guest hydrophobic interaction.

The hydrophobic environment of the interior of sphere **7** is switched by the reversible isomerization of the azobenzene moieties (Figure 8.13). A hydrophobic guest molecule, 1-pyrenecarboxaldehyde, can be incorporated into the sphere in CH_3CN-H_2O (1 : 1) solvent. Because *cis*-azobenzene is more polar than *trans*-azobenzene, the interior of sphere **7** becomes less hydrophobic. Under UV irradiation, the hydrophobic interaction between the sphere and the guests is weakened and the encapsulated guest is expelled outside the sphere. Almost 80% of the azobenzene moieties remain in the *trans* form in the sphere and therefore the guest release is attributed to the polarity change rather than structural change in the sphere. The hydrophobic environment is completely recovered by heating at 50°C and the sphere again takes up the guest.

8.4.7
Peptide-confined Chiral Cages

Enzyme pockets furnish chiral hollow environments where amino acid residues are precisely arranged and asymmetric molecular recognition and chemical transformations are achieved [26]. There are several approaches on the *de novo* design and control of peptide 3D structures [27]. However, the construction of chiral spatial environments from peptides by synthetic means has never been achieved. It is possible to create a library of spheres that tether various kinds of amino acid residues with different lengths (Figure 8.14). $M_{12}L_{24}$ spheres can accommodate up to 96 ($=4\times24$) amino acid residues within the hollows (sphere **8f**), which might be regarded as an artificial "mini-protein". Synchrotron X-ray studies of the sphere **8a** confining 24 L-alanine (L-Ala) residues clarified the endohedral arrangement of the amino acid residues in the sphere (Figure 8.15). Some L-Ala residues are in mutual proximity via the terminal protective groups in the crystalline state.

Aromatic shells of $M_{12}L_{24}$ spheres are highly symmetric and do not have any asymmetric points in themselves. Therefore, the circular dichroism (CD) spectrum of empty sphere shows no peaks. However, in the L-Ala-confined sphere **8a**, chirality of each amino acid is transferred to the spherical shell, displaying a strong negative Cotton effect in the absorption region of the shell (300–350 nm)

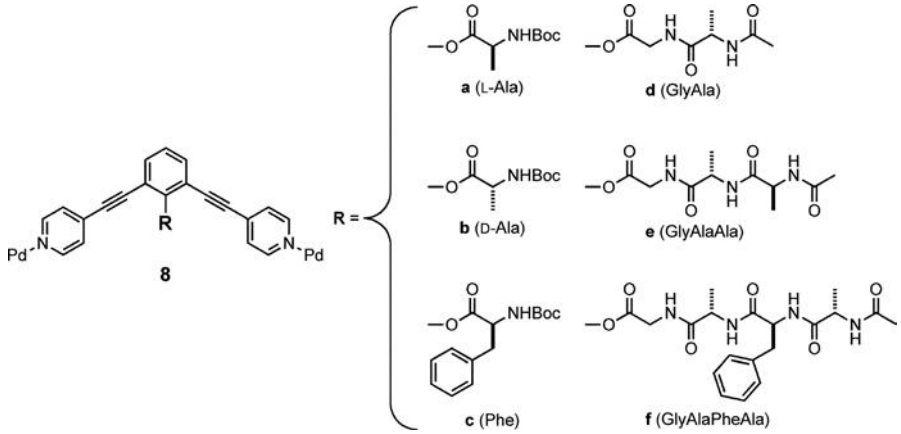

Figure 8.14 Library of peptide-confined $M_{12}L_{24}$ spheres.

(Figure 8.16). The intensity of the induced CD of the sphere is almost 30 times as strong as that of the corresponding ligand. The CD spectra of D/L-Ala-confined spheres have identical shapes and intensities, but opposite signs. The interiors of the spheres where 24 asymmetric centers are accumulated can afford a unique chiral environment. When two kinds of ligands that tether different amino acid residues are used in the formation of the sphere, the internal chiral environment of the obtained sphere should change, depending on the mixing ratio of the two ligands. Although it is difficult to control precisely the ratio and relative positions

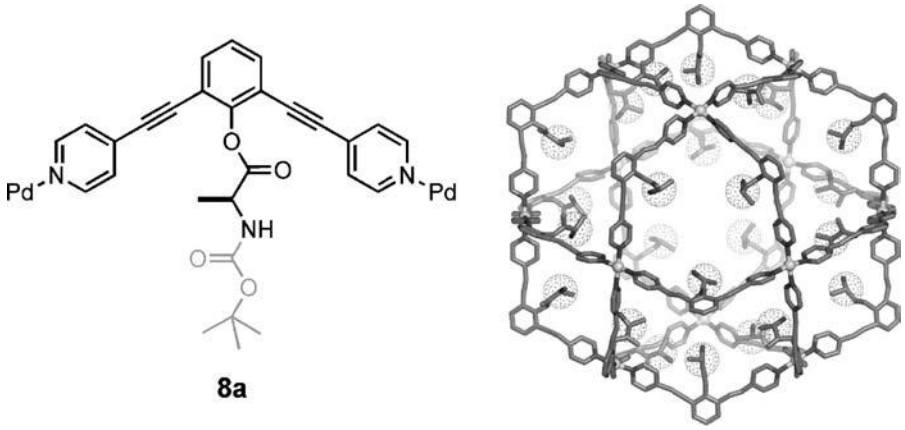

Figure 8.15 X-ray crystal structure of L-Ala-confined sphere **8a**. The terminal Boc groups are disordered and could not be located. Asymmetric centers are shown as dotted spheres.

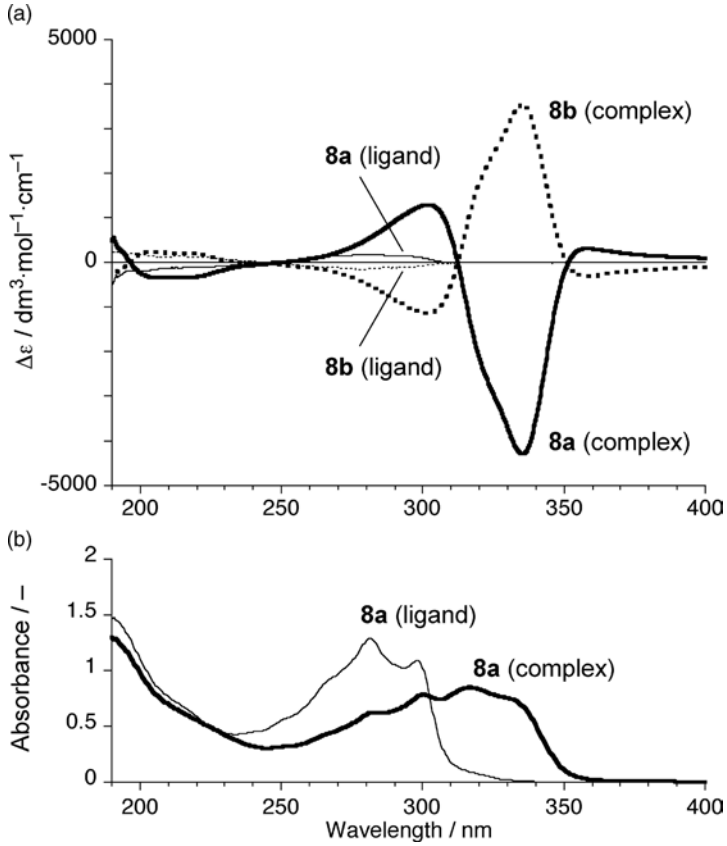

Figure 8.16 (a) CD and (b) UV–Vis spectra of spheres **8a** and **b**. The CD and UV–Vis spectra of the corresponding ligands to spheres **8a** and **b** are also shown as references. Concentration of ligand, 24 μM; concentration of complex, 1 μM.

of the two kinds of ligands introduced, desired peptides can be combinatorially anchored in the sphere. Therefore, the peptide-confined spherical hollows have the potential to be developed as artificial enzyme pockets.

8.5 Conclusions and Outlook

Natural building blocks such as protein-based giant amphiphiles and virus capsides have been redesigned by altering their chemical composition to control precisely the number and position of the introduced functional groups. Molecular self-assembly that is ubiquitously found in biological systems is a powerful method for developing endochemistry of hollow spherical cages. $M_{12}L_{24}$ spherical complexes are versatile

nanosized cages whose internal local environments can be chemically modified on demand. At the stage of ligand designing of $M_{12}L_{24}$ spheres, a desired functionality can be attached to each ligand, resulting in the accurate and efficient introduction of 24 functional groups in the spheres. The positions of functional groups in the spheres are changed by the length of linkers that tether the functional groups to the shells of the spheres. This handling flexibility indicates that the functional groups can be placed at any positions, depending on their molecular sizes. The introduced functional groups are concentrated at the cores of spheres. Therefore, it is possible to develop novel properties and functions that are not otherwise accessible by conventional methods.

Further directions of endohedral functionalization of self-assembled hollow spherical cages are contributions to organic synthesis, materials science and biology. The last topic of peptide-based cages tells us that it is possible to encapsulate biomacromolecules, particularly proteins, to direct the control of biofunctions. The elongation of the pyridyl arms of ligands leads to the expansion of the overall cavity sizes of $M_{12}L_{24}$ spheres. Endochemistry with well-defined spherical cages is just getting started.

References

1 (a) Vriezema, D.M., Aragonès, M.C., Elemans, J.A.A.W., Cornelissen, J.J.L.M., Rowan, A.E. and Nolte, R.J.M. (2005) *Chem. Rev.*, **105**, 1445–1490. (b) Philp, D. and Stoddart, J.F. (1996) *Angew. Chem. Int. Ed. Engl.*, **35**, 1154–1196. (c) Caulder, D.L. and Raymond, K.N. (1999) *Acc. Chem. Res.*, **32**, 975–982. (d) MacGillivray, L.R. and Atwood, J.L. (1999) *Angew. Chem. Int. Ed.*, **38**, 1018–1033. (e) Prins, L.J., Reinhoudt, D.N. and Timmerman, P. (2001) *Angew. Chem. Int. Ed.*, **40**, 2382–2426. (f) Hof, F., Craig, S.L., Nuckolls, C. and Rebek, J. Jr. (2002) *Angew. Chem. Int. Ed.*, **41**, 1488–1508. (g) Seidel, S.R. and Stang, P.J. (2002) *Acc. Chem. Res.*, **35**, 972–983. (h) Fujita, M., Tominaga, M., Hori, A. and Therrien, B. (2005) *Acc. Chem. Res.*, **38**, 369–378.

2 Arora, P.S. and Kirshenbaum, K. (2004) *Chem. Biol.*, **11**, 418–420.

3 (a) Douglas, T. and Young, M. (1998) *Nature*, **393**, 152–155. (b) Douglas, T. and Young, M. (1999) *Adv. Mater.*, **11**, 679–681. (c) Niemeyer, C.M. (2001) *Angew. Chem. Int. Ed.*, **40**, 4128–4158. (d) Flynn, C.E., Lee, S.-W., Peelle, B.R. and Belcher, A.M. (2003) *Acta Mater.*, **51**, 5867–5880. (e) Douglas, T. and Young, M. (2006) *Science*, **312**, 873–875. (f) Singh, P., Gonzalez, M.J. and Manchester, M. (2006) *Drug Dev. Res.*, **67**, 23–41.

4 (a) Chasteen, N.D. and Harrison, P.M. (1999) *J. Struct. Biol.*, **126**, 182–194. (b) Lawson, D.M., Artymiuk, P.J., Yewdall, S.J., Smith, J.M.A., Livingstone, J.C., Treffry, A., Luzzago, A., Levi, S., Arosio, P., Cesareni, G., Thomas, C.D., Shaw, W.V. and Harrison, P.M. (1991) *Nature*, **349**, 541–544.

5 (a) Speir, J.A., Munshi, S., Wang, G., Baker, T.S. and Johnson, J.E. (1995) *Structure*, **3**, 63–78. (b) Reddy, V.S., Natarajan, P., Okerberg, B., Li, K., Damodaran, K.V., Morton, R.T., Brooks, C.L. III and Johnson, J.E. (2001) *J. Virol.*, **75**, 11943–11947.

6 Gillitzer, E., Suci, P., Young, M. and Douglas, T. (2006) *Small*, **2**, 962–966.

7 (a) Kramer, R.M., Li, C., Carter, D.C., Stone, M.O. and Naik, R.R. (2004) *J. Am. Chem. Soc.*, **126**, 13282–13286. (b) Flenniken, M.L., Liepold, L.O., Crowley, B.E., Willits, D.A., Young, M.J. and Douglas, T. (2005) *Chem. Commun.*,

447–449. (c) Douglas, T., Strable, E., Willits, D., Aitouchen, A., Libera, M. and Young, M. (2002) *Adv. Mater.*, **14**, 415–418. (d) Hooker, J.M., Kovacs, E.W. and Francis, M.B. (2004) *J. Am. Chem. Soc.*, **126**, 3718–3719.

8 (a) Zhang, L. and Eisenberg, A. (1995) *Science*, **268**, 1728–1731. (b) Stupp, S.I., LeBonheur, V., Walker, K., Li, L.S., Huggins, K.E., Keser, M. and Amstutz, A. (1997) *Science*, **276**, 384–389. (c) Jenekhe, S.A. and Chen, X.L. (1998) *Science*, **279**, 1903–1907. (d) Won, Y.-Y., Davis, H.T. and Bates, F.S. (1999) *Science*, **283**, 960–963. (e) Förster, S. and Plantenberg, T. (2002) *Angew. Chem. Int. Ed.*, **41**, 688–714. (f) Discher, D.E. and Eisenberg, A. (2002) *Science*, **297**, 967–973. (g) Bucknall, D.G. and Anderson, H.L. (2003) *Science*, **302**, 1904–1905. (h) Jean-François, L. (2006) *Polym. Int.*, **55**, 979–993.

9 O'Reilly, R.K., Hawker, C.J. and Wooley, K.L. (2006) *Chem. Soc. Rev.*, **35**, 1068–1083.

10 (a) Bae, Y., Fukushima, S., Harada, A. and Kataoka, K. (2003) *Angew. Chem. Int. Ed.*, **42**, 4640–4643. (b) O'Reilly, R.K., Joralemon, M.J., Wooley, K.L. and Hawker, C.J. (2005) *Chem. Mater.*, **17**, 5976–5988. (c) O'Reilly, R.K., Joralemon, M.J., Hawker, C.J. and Wooley, K.L. (2006) *Chem. Eur. J.*, **12**, 6776–6786.

11 Tominaga, M., Suzuki, K., Kawano, M., Kusukawa, T., Ozeki, T., Sakamoto, S., Yamaguchi, K. and Fujita, M. (2004) *Angew. Chem. Int. Ed.*, **43**, 5621–5625.

12 Kamiya, N., Tominaga, M., Sato, S. and Fujita, M. (2007) *J. Am. Chem. Soc.*, **129**, 3816–3817.

13 Tominaga, M., Suzuki, K., Murase, T. and Fujita, M. (2005) *J. Am. Chem. Soc.*, **127**, 11950–11951.

14 (a) Horváth, I.T. and Rábai, J. (1994) *Science*, **266**, 72–75. (b) Horváth, I.T. (1998) *Acc. Chem. Res.*, **31**, 641–650.

15 (a) Studer, A., Hadida, S., Ferritto, R., Kim, S.-Y., Jeger, P., Wipf, P. and Curran, D.P.(1997) *Science*, **275**, 823–826. (b) Studer, A., Jeger, P., Wipf, P. and Curran, D.P. (1997) *J. Org. Chem.*, **62**, 2917–2924. (c) Richard, H.F. (1999) *Chem. Eur. J.*, **5**, 1677–1680. (d) Yoshida, J. and Itami, K. (2002) *Chem. Rev.*, **102**, 3693–3716. (e) Zhang, W. (2003) *Tetrahedron*, **59**, 4475–4489.(f) Curran, D.P. (2005) in *Handbook of Fluorous Chemistry*, (eds J.A. Gladysz, D.P. Curran and I.T. Horváth), Wiley-VCH, Weinheim, pp. 101–127.

16 (a) Garcia-Bernabé, A., Krämer, M., Olàh, B. and Haag, R. (2004) *Chem. Eur. J.*, **10**, 2822–2830. (b) Percec, V., Imam, M.R., Bera, T.K., Balagurusamy, V.S.K., Peterca, M. and Heiney, P.A. (2005) *Angew. Chem. Int. Ed.*, **44**, 4739–4745.

17 Sato, S., Iida, J., Suzuki, K., Kawano, M., Ozeki, T. and Fujita, M. (2006) *Science*, **313**, 1273–1276.

18 Pearson, R.G. (1963) *J. Am. Chem. Soc.*, **85**, 3533–3539.

19 (a) Irie, M. (2000) *Chem. Rev.*, **100**, 1685–1716. (b) Fullerton, E.E., Margulies, D.T., Moser, A. and Takano, K. (2001) *Solid State Technol.*, **44**, 87–94. (c) Sun, X., Huang, Y. and Nikles, D.E. (2004) *Int. J. Nanotechnol.*, **1**, 328–346. (d) Tang, Q., Shi, S.-Q. and Zhou, L. (2004) *J. Nanosci. Nanotechnol.*, **4**, 948–963. (e) Tian, H. and Yang, S. (2004) *Chem. Soc. Rev.*, **33**, 85–97. (f) Mayes, E.L. and Mann, S. (2005) in *Nanobiotechnology*, (eds C.M. Niemeyer and C.A. Mirkin), Wiley-VCH, Weinheim, 278–287. (g) Naito, K., Hieda, H., Ishino, T., Tanaka, K., Sakurai, M., Kamata, Y., Morita, S., Kikitsu, A. and Asakawa, K. (2005) in *Progress in Nano-Electro-Optics III*, (ed. M. Otsu), Springer, Berlin, 127–144.

20 (a) Farina, M. (1988) in *Encyclopedia of Polymer Science and Engineering*, (ed. J.I. Kroschwitz), Wiley, New York, Vol. 12, 486–504. (b) Miyata, M. (1996) in *Comprehensive Supramolecular Chemistry*, (ed. D. Reinhoudt), Pergamon Press, Oxford, Vol. 10, 557–582. (c) Moller, K. and Bein, T. (1998) *Chem. Mater.*, **10**, 2950–2963. (d) Tajima, K. and Aida, T. (2000) *Chem. Commun.*, 2399–2412.

(e) Cardin, D.J. (2002) *Adv. Mater.*, **14**, 553–563.

21 (a) Uemura, T., Kitagawa, K., Horike, S., Kawamura, T., Kitagawa, S., Mizuno, M. and Endo, K. (2005) *Chem. Commun.*, 5968–5970. (b) Uemura, T., Kitaura, R., Ohta, Y., Nagaoka, M. and Kitagawa, S. (2006) *Angew. Chem. Int. Ed.*, **45**, 4112–4116. (c) Uemura, T., Horike, S. and Kitagawa, S. (2006) *Chem. Asian J.*, **1**, 36–44.

22 Murase, T., Sato, S. and Fujita, M. (2007) *Angew. Chem. Int. Ed.*, **46**, 1083–1085.

23 (a) Kumar, G.S. and Neckers, D.C. (1989) *Chem. Rev.*, **89**, 1915–1925. (b) Natansohn, A. and Rochon, P. (2002) *Chem. Rev.*, **102**, 4139–4175. (c) Dugave, C. and Demange, L. (2003) *Chem. Rev.*, **103**, 2475–2532. (d) Yager, K.G. and Barrett, C.J. (2006) *J. Photochem. Photobiol. A*, **182**, 250–261.

24 (a) Wang, G., Tong, X. and Zhao, Y. (2004) *Macromolecules*, **37**, 8911–8917. (b) Tong, X., Wang, G., Soldera, A. and Zhao, Y. (2005) *J. Phys. Chem. B*, **109**, 20281–20287. (c) Lee, H., Pietrasik, J. and Matyjaszewski, K. (2006) *Macromolecules*, **39**, 3914–3920. (d) Liu, X. and Jiang, M. (2006) *Angew. Chem. Int. Ed.*, **45**, 3846–3850.

25 Murase, T., Sato, S. and Fujita, M. Angew. (2007) *Chem. Int. Ed.*, **46**, 5133–5136.

26 (a) Adams, M.J., Buehner, M., Chandrasekhar, K., Ford, G.C., Hackert, M.L., Liljas, A., Rossmann, M.G., Smiley, I.E., Allison, W.S., Everse, J., Kaplan, N.O. and Taylor, S.S. (1973) *Proc. Natl. Acad. Sci. USA*, **70**, 1968–1972. (b) Auerbach, G., Ostendorp, R., Prade, L., Korndörfer, I., Dams, T., Huber, R. and Jaenicke, R. (1998) *Structure*, **6**, 769–781. (c) Read, J.A., Winter, V.J., Eszes, C.M., Sessions, R.B. and Brady, R.L. (2001) *Proteins: Struct. Funct. Genet.*, **43**, 175–185.

27 (a) Blanco, F.J., Jimenez, M.A., Herranz, J., Rico, M., Santoro, J. and Nieto, J.L. (1993) *J. Am. Chem. Soc.*, **115**, 5887–5888. (b) Haque, T.S. and Gellman, S.H. (1997) *J. Am. Chem. Soc.*, **119**, 2303–2304. (c) Peczuh, M.W., Hamilton, A.D., Sánchez-Quesada, J., Mendoza, J., Haack, T. and Giralt, E. (1997) *J. Am. Chem. Soc.*, **119**, 9327–9328. (d) Kelso, M.J., Hoang, H.N., Oliver, W., Sokolenko, N., March, D.R., Appleton, T.G. and Fairlie, D.P. (2003) *Angew. Chem. Int. Ed.*, **42**, 421–424. (e) Tashiro, S., Tominaga, M., Yamaguchi, Y., Kato, K. and Fujita, M. (2006) *Angew. Chem. Int. Ed.*, **45**, 241–244. (f) Tashiro, S., Kobayashi, M. and Fujita, M. (2006) *J. Am. Chem. Soc.*, **128**, 9280–9281.